Send Orders for Reprints to reprints@benthamscience.ae

Current Organic Chemistry, 2015, *19*, 000-000

Hierarchically Organized Nanocomposites Derived from Low-dimensional Nanomaterials for Efficient Removal of Organic Pollutants

Yue-E Miao, Yunpeng Huang, Chao Zhang and Tianxi Liu*

State Key Laboratory of Molecular Engineering of Polymers, Department of Macromolecular Science, Fudan University, Shanghai 200433, P. R. China

Tianxi Liu

Abstract: Low-dimensional nanocarbon materials and metal/metal oxide (hydroxide) or semiconductors have been world-widely investigated due to their distinct physical and chemical properties for potential applications in environmental remediation. Three-dimensional (3D) hierarchical nanocomposites can be facilely constructed by using different low-dimensional nanomaterials as building blocks, thus leading to the full utilization or even synergistic effect of all the component materials with multifunctional properties. Herein, an overview is presented on the design and construction of hierarchically organized nanocomposites derived from low-dimensional nanocarbons (*i.e.* one-dimensional (1D) carbon nanotubes (CNTs), two-dimensional (2D) graphene, and 3D aerogels) and metal, metal oxide (hydroxide) or semiconductors (*i.e.* 0D nanoparticles (NPs), 1D nanorods, nanowires, nanotubes or nanofibers, 2D flakes), and their potential applications for efficient removal of organic pollutants through adsorption or catalytic reactions.

Keywords: Hierarchical organization, low-dimensional, metal/metal oxides, nanocarbons, organic pollutant removal.

1. INTRODUCTION

The increasing by-products deriving from the rapid pace of industrialization have posed a major health risk to humankinds by producing hazardous wastes, poisonous gas fumes and smokes to the environment. Water purification technology has become an urgent environmental and public health problem due to the severe contamination by organic pollutants (*e.g.*, methyl orange, methylene blue, and rose red), heavy metal ions (*e.g.*, Pb^{2+}, Cr^{3+}, and Cd^{2+}), microorganisms (*e.g.*, *Escherichia coli* (*E. coli*), and *Staphylococcus aureus* (*S. aureus*)) [1, 2]. Nanomaterials, such as metals, metal oxides (hydroxides), semiconductors, and carbon materials are excellent adsorbents and catalysts for environmental remediation owing to their large specific surface area and high reactivity. Moreover, densely distributed low-coordinated atoms can be found at surfaces and edges of nanomaterials with reduced size and large curvature radii, which endows them with a surface that is highly reactive in adsorbing and degrading pollutants in water and air [3-5]. Nanomaterials with different shapes/morphologies/forms can be fabricated through various approaches, such as mechanical alloying techniques, chemical sol-gel methods, gas-phase synthesis techniques, physical or chemical vapor deposition, and microwave techniques [6]. However, self-aggregation issues are inevitably aggravated due to the high surface energy of these nanoparticles (NPs) with small sizes, which results in the obstacle in preparing stable, well-dispersed and easy-recovered suspensions for practical environmental systems [7, 8]. To overcome the limitations of easy aggregation and improve the surface and optical properties of NPs, design and construction of novel nanocomposites has gained research attentions.

With various excellent materials created by nature during the evolution process, hierarchical organization of low-dimensional building blocks into biomimetic structures is considered as an alternative approach for preparation of next-generation materials [9, 10]. Three-dimensional (3D) hierarchical nanocomposites can be facilely obtained by the fine assembly of different low-dimensional nanomaterials (*e.g.*, zero-dimensional (0D) nanoparticles (NPs), one-dimensional (1D) nanofibers, nanowires, or nanotubes, and two-dimensional (2D) nanoplatelets, or flakes) as building blocks, which definitely will make full uses of all the component materials, or even result in unexpected multifunctional properties and applications [11, 12]. Nanocarbon materials (*i.e.*, 1D carbon nanotubes (CNTs), 2D graphene, and 3D aerogels) and metal/metal oxide (hydroxide) or semiconductors with different dimensions (*e.g.*, 0D NPs, 1D nanotubes, nanowires or nanofibers, and 2D flakes) have been world-widely investigated due to their unique but distinguishing physical and chemical properties for various applications in solar cells, supercapacitors, lithium ion batteries, sensors, and water treatment [13, 14]. Especially, nanocarbons with much higher surface area than the traditional activated carbons, have emerged as key materials for designing experimental water treatment strategies owing to their aforementioned excellent physical, chemical and electronic properties. 3D composite architectures assembled from 1D CNTs and 2D graphene can better utilize the performance of graphitic carbon materials in environmental applications [15, 16]. On the other hand, due to their compositional and morphological variability, facile preparation, low cost, high reactivity toward adsorption or catalytic removal of organic pollutants, low-dimensional metal, metal oxide (hydroxide) or semiconductors have been widely used for environmental applications [17]. Herein, we will give an overview of the design and construction of hierarchically organized nanocomposites derived from low-dimensional nanocarbons (*i.e.*, 1D CNTs, 2D graphene, 3D aerogel) and metal/metal oxide (hydroxide) or semiconductors (*i.e.*, 0D nanoparticles (NPs), 1D nanorods, nanowires, nanotubes or nanofibers, 2D flakes), and illustration of their potential applications for efficient removal of organic pollutants.

*Address correspondence to this author at the State Key Laboratory of Molecular Engineering of Polymers, Department of Macromolecular Science, Fudan University, Shanghai 200433, P. R. China; Tel: +86-21-55664197; Fax: +86-21-65640293; E-mail: txliu@fudan.edu.cn;

1385-2728/15 $58.00+.00

2. ONE-DIMENSIONAL BUILDING BLOCK BASED NANOCOMPOSITES FOR REMOVAL OF ORGANIC POLLUTANTS

2.1. CNTs Based Nanocomposites

Owing to the unique 1D hollow and layered structures, high specific surface area, good chemical, thermal, and mechanical properties, CNTs show great potentials in various applications including high-performance solar cells, sensors, next generation transistors, and water-treatment fields, such as sorbents, catalyst, or filters since its discovery by Iijima in 1991 [18-20]. Among them, CNTs have been widely applied as nanoadsorbents for removing a variety of pollutants, *e.g.* heavy metal ions and organic dyes [21, 22]. Because of the hydrophobic nature of their outer surfaces, CNTs have a strong affinity to organic chemicals, especially to nonpolar organic compounds, such as naphthalene, phenanthrene, and pyrene [23, 24]. Surface chemistry is an important factor influencing the adsorption behavior of CNTs. Functional groups such as -OH, -C=O and -COOH are intentionally introduced onto CNT surfaces by acid oxidation or air oxidation, which makes it more hydrophilic and suitable for the adsorption of organic contaminants [25-27]. Despite the numerous benefits, the widespread applications of CNTs for water treatment are still limited for its high cost of production. Thus, CNTs, with good chemical stability and large surface area, should be used as a support to be integrated with varying functionalities to form composite materials, which can greatly facilitate the dispersion of nanoparticles to enable the synergistic effect of each component, as well as reduce the cost in production [28, 29]. Chemical treatment has been considered as an effective strategy to introduce functional groups on the surface of CNTs, thus to achieve uniformly distributed catalytic nanoparticles on CNTs [30, 31]. Whereas, it's difficult to realize accurate controllability, thus resulting in new approaches of physical evaporation, atomic layer deposition, electroless deposition, and hydrothermal reactions, to get highly dispersed nanoparticles on 1D CNTs [29]. Therefore, the facile construction of hierarchical nanocomposites based on 1D CNTs and low-dimensional NPs can easily realize the greatly enhanced adsorption or photocatalytic properties for water remediation applications.

Metal NPs of zero dimensions, such as silver (Ag), copper (Cu), iron (Fe), cobalt (Co) and nickel (Ni), are paid much attentions due to their high catalytic activity, lost cost and good recyclability [32]. Highly monodispersed Ag NPs (about 5 nm) have been deposited on multi-walled carbon nanotubes (MWNTs) with different Ag contents as shown in Fig. **1** [33]. Attributed to the good dispersion of Ag NPs on MWNT surface, the as-prepared Ag/MWNT composites exhibited highly electrocatalytic activity towards hydrazine oxidation. Besides, broad-spectrum biocidal activity has been achieved toward many different bacteria, fungi, and viruses. Jung *et al.* reported the preparation of Ag-coated MWNT hybrid nanoparticles (Ag/MWNTs) using aerosol nebulization and thermal evaporation/condensation processes [34]. Due to the successful attachment of Ag NPs onto MWNT surfaces, the antimicrobial activity of Ag/MWNT against bacterial bioaerosols was effectively enhanced compared with that of MWNTs or Ag NPs alone, being promising for applications in antibacterial control systems. Similarly, Ag@AgBr/CNT nanocomposite with visible-light-harvesting property was independently obtained by photoreduction of AgBr/CNT [35]. Electrochemical impedance spectroscopy (EIS) testing suggested that higher charge transporting efficiency is obtained for longer CNTs than shorter ones in Ag@AgBr/CNT, well agreed with the visible-light photocatalytic reduction trend (Ag@AgBr/CNT-L > Ag@AgBr/CNT-M > Ag@AgBr/CNT-S) towards CO_2. Lu *et al.* investigated the use of Co/Al_2O_3, Fe/Al_2O_3, and Ni/Al_2O_3 catalysts for growth of CNTs, where CNTs with a diameter of 20 nm have been obtained and, vice versa, used as a support for the growth of Co particles with sizes smaller than 10 nm [36]. The Co/CNT catalyst showed high removal efficiency of 70%-90% and 60-80% for BTEX (*i.e.*, benzene, toluene, ethylbenzene, and xylene) and PAHs (*i.e.*, polycyclic aromatic hydrocarbons), respectively. Furthermore, efficient removal of NO (82%), CO (70%), and SO_2 (55%) was simultaneously achieved for the Co/CNT catalyst.

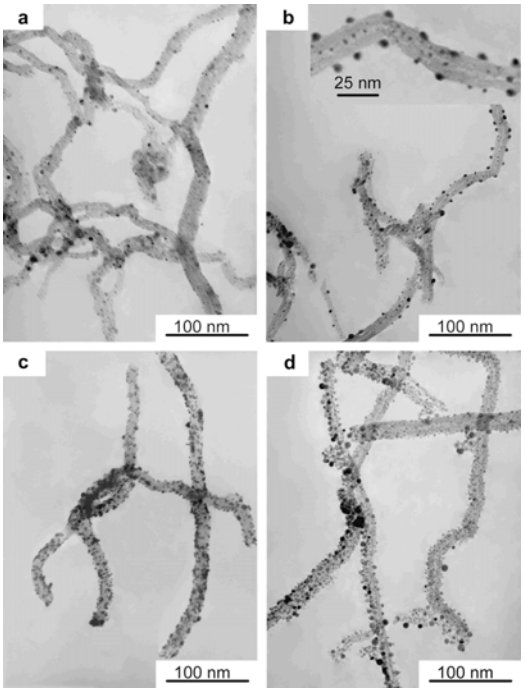

Fig. (1). Transmission electron microscopy (TEM) images of Ag/CNT composites with different Ag contents: 10% (a), 20% (b) (inset: enlarged image of panel b), 40% (c), and 60% (d) [33].

With good electronic conductivity, high surface areas and adsorption capacities, CNTs are good supports as well as dopants for semiconductive oxides, such as TiO_2 and ZnO, in photocatalytic degradation of organic pollutants, due to the effective cooperation between CNTs and metal oxides [17]. For example, aqueous pollutants including dyes [37, 38], benzene derivatives [39], and carbamazepine were efficiently photodegraded by CNT/TiO_2 composites [40]. More practically, CNT/TiO_2 composite has found application in the degradation of nitro phenols from real wastewater under sunlight and the composite held repetitive photocatalytic activity [41]. In Yu's study, aligned MWNTs with well-graphited walls coated with TiO_2 nanoparticles were fabricated on a titanium foil by atmospheric pressure chemical vapor deposition. The TiO_2-MWNT heterojunction could minimize recombination of photoinduced electrons and holes at the MWNTs-semiconductor interface, and had a more effective photoconversion capability than aligned TiO_2 nanotubes on titanium substrate (TiO_2/Ti) [42]. Similarly, a modified sol-gel method was applied to prepare TiO_2 and MWNT composites, which surprisingly exhibited visible-light activity although TiO_2 is only UV active for its wide bandgap (3.2 eV) [43]. Wonderfully, the possible formation of Ti-C and Ti-O-C structures where carbon atoms substituted for both oxygen and titanium atoms in TiO_2 lattice was observed by X-ray photoelectron spectroscopy

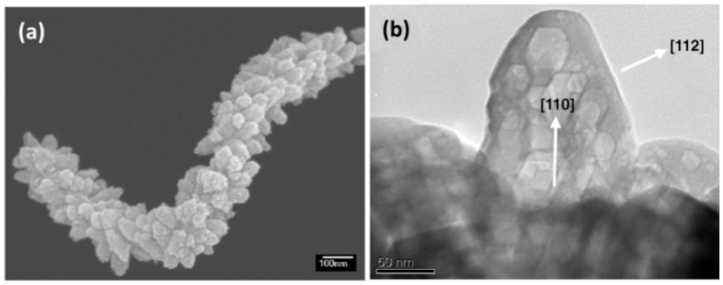

Fig. (2). Field-emission scanning electron microscopy (FESEM) image of a single strand of mesoporous TiO_2/CNTs nanocomposite (a); Transmission electron microscopy (TEM) image of rutile TiO_2 product obtained from TiO_2/CNTs nanocomposite (b) [45].

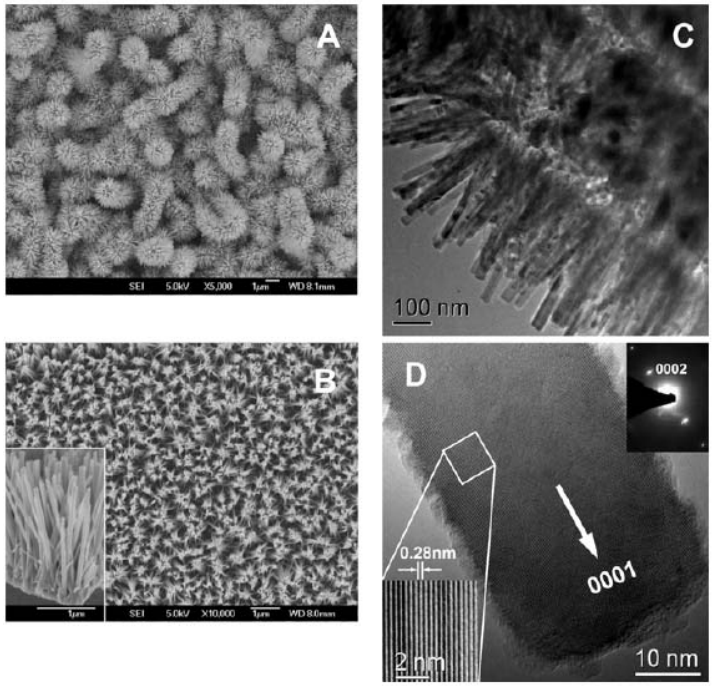

Fig. (3). Top view SEM images of ZnO-NW/MWNT (A) and ZnO-NW arrays on a Ta foil. The inset in panel B shows the side view of ZnO-NWs (B). TEM image of ZnO nanowires on MWNTs (C), and high-resolution TEM image of ZnO nanowire (D) [47].

(XPS), which were responsible for the extra photo absorption and photoelectrocatalytic (PEC) activity under visible-light illumination [17]. Aiming to achieve CNT-TiO_2 in a more controllable way, atomic layer deposition technique has been adopted to deposit TiO_2 on MWNTs. By combining with analytical transmission electron microscopy techniques, it accurately characterized the CNT-TiO_2 interface and offered a good control of the size, crystallinity and morphology of TiO_2 on CNTs [44]. One-pot chemical approach has also been applied in preparation of 1D mesocrystals of anatase TiO_2 onto 1D MWNTs (Fig. **2**), which exhibited high photoactivity for methyl orange degradation [45]. This should be ascribed to the large specific area of porous TiO_2 phase, and the highly oriented attachment of TiO_2 nanocrystallites on the conductive CNT support, which can inhibit the recombination of electron/hole pairs by forming electron reservoirs. Therefore, although with no photoactivity, CNTs are excellent supporting substrates for other semiconductors as efficient 1D photocatalysts for their outstanding optical and electrical properties.

Vietmeyer *et al.* reported ZnO nanoparticles decorated functionalized single-walled carbon nanotubes (SWNTs) to quantitatively analyze the charge separation and transportation properties [46]. Highly improved photoconversion efficiency was achieved for photoelectrochemically active ZnO/SWNT nanocomposite films compared to that of mesoscopic ZnO films. Fast charge separation and electron injection rate constant of 1×10^8 s^{-1} also occurs in the heterojunction of 1D ZnO nanowires (ZnO-NWs) and 1D MWNT arrays, where ZnO-NWs were adhesively grown on MWNT arrays by a hydrothermal process (Fig. **3**) [47]. Linear sweep voltammetry and amperometry revealed remarkably increased charge transfer rate of ZnO-NW/MWNT nanocomposite over pure ZnO-NWs, with the Mott-Schottky plot displaying a high donor density of 3.9×10^{19} cm^{-3}, a flat band potential of -0.8 V, and a space charge layer of 7 nm. In addition, ZnO-NW/MWNT nanocomposite yields a higher photocurrent and lower decay constant than pure ZnO-NWs, which is attributed to the hindered and retarded electron/hole pair recombination in ZnO-NW/MWNT heterojunction. Thus, it affords potential applications for photocatalysis and photoelectrical devices. Closely attached ZnS nanocrystals on CNTs were also prepared, to achieve efficiently improved interfacial electron transfer was and restrained electron/hole pair recombination of ZnS [48]. The effectively increased photocatalytic activity of ZnS nanocrystals by carbon nanotubes again demonstrates that large supporting surface areas as well as spatial confinement are fully achieved by the facile construction of 1D CNTs and 0D or 1D semiconductors, which could provide abundant reaction sites for high exposure to light, thus leading to faster degradation reaction rates.

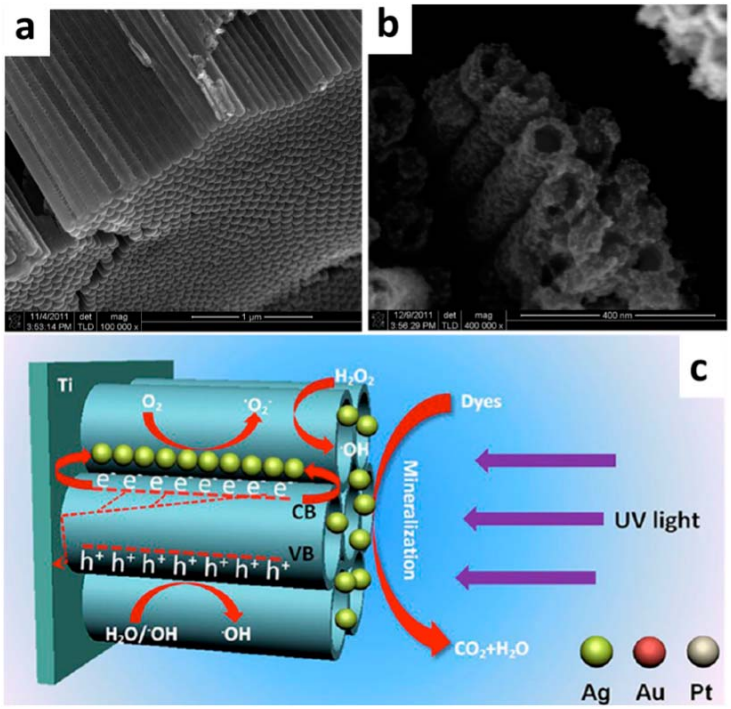

Fig. (4). SEM image of the titania nanotube (TNT) array substrate (a); top-view SEM image of the Pt/TNT hybrid nanostructures prepared via the LBL self-assembly approach (b); pictorial representation of the proposed mechanism for the photocatalytic degradation of dye pollutant over the M/TNT (M = Au, Ag, Pt) heterostructures (c) [61].

2.2. 1D Metal Oxide Nanostructure Based Composites

With higher specific surface area and pore volume, facilitated long-distance electron transport, and markedly enhanced light absorption and scattering of 1D geometry as compared to their bulk materials, studies of 1D nanostructures have experienced an exponential growth in recent years for potential applications in photocatalysis [49-52]. Being an attractive semiconductor, 1D TiO_2 nanostructures have been obtained by various approaches for non-selective photodegradation of organic pollutants [29]. Fujishima and coworkers reported the preparation of TiO_2 nanotube arrays with good alignment by electrochemical anodization for photocatalytic degradation of gaseous acetaldehyde molecules in air [53]. Remarkably enhanced degradation rate can be observed with the increasing lengths of TiO_2 nanotubes arrays, which speculatively explains for the length effect on photoactivity of TiO_2 nanotube arrays. ZnO nanotubes also have been reported by Wang's group via a low-temperature Ga-catalyzed vapor transport approach, which proposes a vapor-liquid-solid process from the root of the nanotube [54]. However, the narrow absorption spectra, low quantum efficiency, and possible photodegradation of photocatalyst still limit the utilization of single phase nanostructures. To avoid the problems of single-phase 1D nanostructures, multi-component nanocomposites have been successively developed.

Due to the synergistic effect between different compounds, heterostructures play an important role in enhancing photo-induced catalytic reactions [55-57]. Mesoporous TiO_2 (B) nanowires (TNWs(B)) supported Fe_2O_3 NPs has been reported by a facile impregnation-solvothermal method, in which the open porous structure of TNWs(B) provided a confined micro-environment for well dispersion of Fe_2O_3 NPs [58]. The photocatalytic experiments showed remarkable catalytic activity of Fe_2O_3/TNWs(B) for photochemical oxidation of Direct Red 4BS in presence of H_2O_2, as well as excellent tolerance to organic matter poisoning, which may be ascribed to favorable synergetic effect of Fe_2O_3 NPs and TNWs(B) support. With Sb:SnO_2@TiO_2 nanobelt electrode serving as a conductive template, 3D Sb:SnO_2@TiO_2-$SrTiO_3$ heterostructures has been demonstrated through a facile hydrothermal process [59]. The Fermi level shift and blocked layer effect by $SrTiO_3$ result in higher onset potential, saturated photocurrent and significantly enhanced photocatalytic degradation of methylene blue for Sb:SnO_2@TiO_2-$SrTiO_3$ heterostructure in comparison to Sb:SnO_2@TiO_2 nanostructure, which further manifests synergetic effect on enhanced PEC and photocatalytic performance from the 3D heterojunction architectures. By utilizing oppositely charged polyelectrolytes, nanocomposites of noble metal/1D semiconductors were easily obtained by a layer-by-layer (LBL) self-assembly route (Fig. **4a**, **4b**) [60-63]. Remarkably enhanced photo-degradation activity towards organic dyes has been achieved for the integrated heterostructures afforded by multilayering polyelectrolytes, where the "electron reservoir" of metal NPs effectively prolongs the lifetime of photogenerated electron/hole charge carriers (Fig. **4c**). Thus, the LBL self-assembly method provides a simple approach for construction of regularly arranged metal/1D semiconductor hybrid nanostructures.

Electrospinning is a simple technique to produce 1D nanofibers with submicron diameter, which possess outstanding properties of high specific surface area and porosity for potential applications in sensors, catalysts, as well as ultrafiltration and separation membranes [64, 65]. Therefore, electrospun nanofibers are considered as promising matrix or template for a variety of hierarchical nanostructures in environmental remediations [66-69]. A novel heterogeneously arranged TiO_2/$CoFe_2O_4$ nanofiber catalysts was obtained by combination of sol-gel process, electrospinning, and high-temperature treatment [70]. Both of enhanced UV-light absorbance and broadened visible-light response region are observed in the

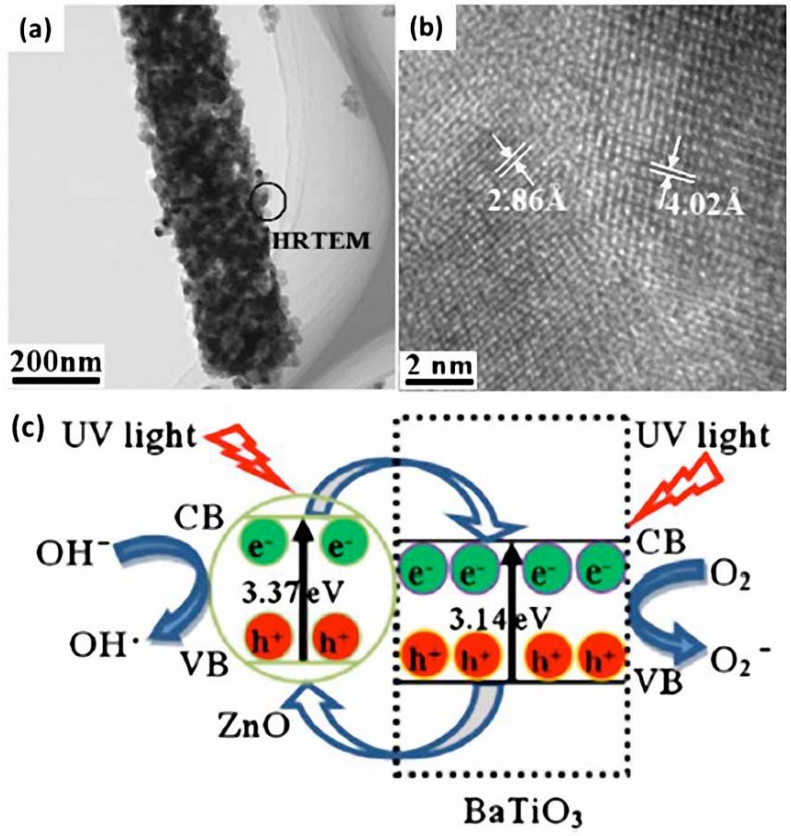

Fig. (5). TEM (a) and high-resolution TEM (b) images of $ZnO/BaTiO_3$ nanofiber heterostructures. Schematic diagram of photocatalytic mechanism in aqueous solution for $ZnO/BaTiO_3$ nanofiber heterostructures (c) [74].

presence of $CoFe_2O_4$, thus achieving high removal efficiency (95.87%) toward methylene blue, being approaching that of Degussa P25. Besides, the magnetically separable property could effectively avoid the secondary pollution as well as endow these fibers with multi recyclability and reusability. Using thiourea and CS_2 as the sulfur precursors, S-doped TiO_2 nanofibershave been prepared via electrospinning technique, which effectively inhibited the crystalline grain size and notably increased the visible-light absorbance [71]. Similarly, CdS/TiO_2 NPs-decorated carbon nanofibers were introduced as a novel photocatalyst working under visible light radiation for the effective hydrolytic dehydrogenation of ammonia borane [72]. The favorable electron-transfer properties, better dispersion, high surface area, and adsorption property are the main features of nanocomposites that exhibit high catalytic efficiency. N-doped ZnO nanonodules decorated SnO_2 hybrid nanofibers were also prepared by phase-separated co-electrospinning of poly(acrylonitrile) (PAN) and poly(vinylpyrrolidone) (PVP) composites, followed by calcination to hybrid semiconductor metal oxide (SMO) and replacing the oxygen atom with nitrogen atom [73]. By precisely adjusting the concentration of precursor PVP, increased photocatalytic activity of hybrid SMO nanofibers can be achieved with increasing ZnO nanonodules. Ascribed to the increased surface and interfacial area of the heterostructure, it provides an effective approach for synthesizing inorganic hybrids with core-shell nanostructures in catalytic applications.

Surface modification has been paid much attention for its diversity in building hierarchical micro/nanostructures. Uniformly distributed ZnO nanoparticles on primary $BaTiO_3$ nanofibers ($ZnO/BaTiO_3$ nanofiber heterostructures) have been facilely obtained by combination of electrospinning and a hydrothermal process (Fig. **5a**, **5b**) [74]. Ascribed to the synergistic effects of high specific surface area and effective photogenerated electron/hole pair separation, $ZnO/BaTiO_3$ nanofiber heterostructures exhibited better photocatalytic performance compared with pure ZnO powders (Fig. **5c**). Shang *et al.* also reported the preparation of a branched nanofiber-nanorod fabric (TiO_2/NiO, TiO_2/ZnO, and TiO_2/SnO_2) with hierarchical heterostructures by a generalizable approach of combining electrospinning with hydrothermal method (Fig. **5**) [75]. Photocurrent and photocatalytic studies suggest that enhanced photocatalytic activity deriving from the higher charge carrier mobility can be achieved for branched hierarchical heterostructure fabric compared to bare TiO_2 nanofibrous mat under light irradiation, which demonstrates the possible realization of a new class of nano-heterostructured fabrics with unique optical and catalytic properties.

For easy recovery and recyclability, highly flexible electrospun SiO_2 fiber membrane is considered as an ideal matrix for further surface modification, such as physical vapor deposition, hydrothermal treatment, or surface grafting. Hierarchically structured 1D ZnO/1D SiO_2 composite fiber membranes with high flexibility have been obtained through epitaxial growth of ZnO nanorods on SiO_2 fibers, exhibiting efficient photocatalytic and recycling ability towards organic dyes [76]. Similarly, greatly improved adsorption efficiency towards organic dyes and microorganisms could be realized by the uniform distribution of 2D γ-AlOOH (Boehmite) nanoplatelets on surface of 1D SiO_2 fibers [77]. Liu *et al.* reported polyaniline (PANI) coated TiO_2/SiO_2 nanofiber membranes by a combination of electrospinning, calcination and in situ polymerization [78]. Photocatalytic degradation tests show the as-prepared nanofiber membranes exhibit enhanced photocatalytic activity for visible-light degradation of methyl orange, which can be attributed to the

synergistic effect of PANI and TiO_2. Furthermore, it is very easy to handle the free-standing membrane, making it promising for potential applications in photocatalysis.

3. TWO-DIMENSIONAL BUILDING BLOCK BASED NANOCOMPOSITES FOR REMOVAL OF ORGANIC POLLUTANTS

3.1. Graphene Based Nanocomposites

With theoretical surface area of 2630 m^2 g^{-1}, high electrical conductivity (10^6 S cm^{-1}), strong mechanical properties, excellent thermal conductivity (~ 5000 W m^{-1} K^{-1}), and absorption of 2.3% light for each layer, two-dimensional graphene sheet has been considered as one of the greatest novel materials for potential applications in electronics, optoelectronics, environmental and biomedical applications [79-81]. Moreover, the high surface area and pore volume, as well as the presence of surface functional groups make graphene good adsorbents for water purification [82-84]. The hybridization of inorganic nanoparticles in 2D graphene nanocomposites can effectively prevent graphene aggregation, as well as to achieve a hierarchical structure with high surface area and pore volume for efficient removal of dyes as well as other organic contaminants [85]. Therefore, the construction of 2D graphene based hierarchical nanocomposites can be used as general platforms for removal of hazardous species in environment.

Due to the non-toxicity, cheap and easy production, capability of degrading a wide range of organic contaminants, zero-dimensional (0D) zero-valent iron (ZVI) has intrigued a great deal of research since the discovery of bulk zero-valent iron (ZVI) for ground water remediation by Gillham and O'Hannesin [8]. However, the high surface energy and strong magnetic interactions of ZVI make it still remains a great challenge to prepare stable and well-dispersed ZVI suspensions for practical environmental systems [86, 87]. To address these issues, controllable synthesis of hierarchical nanocomposites derived from ZVI and supporting graphene materials has been realized to achieve a synergic combination of ZVI with the supporting materials [88]. By using graphene oxide (GO) as a supporting matrix, Fe nanoparticles@graphene composites (FGC) are synthesized in which Fe^{3+}@GO complexes are reduced into Fe and graphene simultaneously by $NaBH_4$ solution [89]. The as-formed FGC hybrid composites exhibit high removal capacities of methyl blue due to the reduced particle size, inhibited aggregation and increased adsorption sites of Fe nanoparticles. Magnetic graphene-Fe_3O_4@carbon (GFC) hybrids also have been synthesized for removal of organic dyes [90]. 2D graphene sheets can efficiently prevent the aggregation to achieve highly dispersed Fe_3O_4 nanoparticles with enhanced specific surface area, while the carbonaceous layer effectively protects Fe_3O_4 nanoparticles in acidic environments. Thus, rapid and efficient adsorption is achieved, suggesting the potential applications of GFC hybrids in removal of organic dyes. Xiong *et al*. reported the preparation of copper-ion-modified reduced graphene oxide (RGO) composites, in which excited electrons are continuously passed from RGO sheets to adsorbed oxygen by the "electron relay" of copper species to generate continuous reactive oxygen species, thus resulting in greatly enhanced degradation of rhodamine B (RhB) [91]. In the same way, Ni@RGO nanocomposites obtained from hydrothermally synchronous reduction of GO and Ni^{2+} ions also exhibit enhanced ferromagnetic behavior, as well as high removal efficiency of organic dye molecules comparison with bulk nickel [92]. 1D Ag/AgCl and graphene oxide hybridized nanocomposites, Ag/AgCl/GO, also have been easily obtained by involving GO nanosheets in the oxidation-chloridization procedure of prefabricated 1D Ag nanowires [93]. The enhanced photocatalytic activity of Ag/AgCl/GO nanocomposites over Ag/AgCl nanostructures indicates the cooperative or synergistic effects between intrinsic 1D Ag/AgCl nanostructures, and efficient charge separation provided by GO nanosheets for better adsorption of methyl orange molecules.

To further enhance the reactivity of ZVI, bimetallic nanoparticles with a thin layer of transition metals deposited on the surface of iron, such as Pd, Cu, Ni or Ag, have been developed for effective removal of contaminants. Huang *et al*. found that the dechlorination rate of tetrachlorobisphenol A by Pd/Fe bimetallic particles was more rapid than that by ZVI, which is believed to be enhanced by the transition metal doping that serves as hydrogen catalysts or reactive electron donors [94]. However, it still remains a great challenge to obtain highly efficient dehydrogenation catalysts due to the strong magnetism and aggregation. Therefore, weak-branched polyethyleneimine was applied in the deposition of Fe-Ni NPs on GO by a simple co-reduction method [95]. A 18 times faster dehydrogenation rate, with 982 mL min^{-1} g^{-1} at 293 K towards the hydrolysis of ammonia borane, has been observed for Fe-Ni NPs on PEI-decorated GO compared to Fe-Ni NPs directly deposited on GO, being promising for substituting platinum catalyst under the same conditions.

Cadmium sulfide (CdS) has attracted much attentions for its band gap (2.4 eV) in well accordance with the spectrum of sunlight, chemical stability, easy and inexpensive synthesis through various reproducible methods [96]. However, it still remains great challenge to improve the charge separation efficiency, and retrieve CdS nanoparticles from treated as well. To overcome the above drawbacks, construction of heterostructures by 2D graphene and 0D or 1D CdS has been demonstrated to be a potential approach due to the large surface area and extraordinarily conductive sp^2-hybridized carbon network of graphene [97, 98]. The photo-corrosion of CdS and leaching of Cd^{2+} can be effectively inhibited by the interactions between GO sheets and CdS nanoparticles, thus resulting in much improved efficiency in visible-light photodegradation of water pollutants over pure CdS nanoparticles [99]. Yu *et al.* also reported zinc sulfide-graphene (ZnS-GR) nanocomposites with uniformly dispersed ZnS quantum dots (QDs) by a simple solvothermal strategy, which exhibit much higher photoactivity towards degradation of methylene blue than nanoparticle crystal ZnS (NPC-ZnS) due to particularly high specific surface area and electron conductivity of graphene [100]. CdS nanowires-reduced graphene oxide nanocomposites (CdS NW-RGO NCs) combining 1D with 2D nanostructures are also successfully achieved via the combination of electrostatic self-assembly and hydrothermal reduction processes (Fig. **6A**, **6B**) [101]. Significantly enhanced selective visible-light reduction of aromatic nitro organics was observed for CdS NW-RGO compared with CdS nanowires (CdS NWs) (Fig. **6C**, **6D**), offering new windows for fabrication and applications of various specific 1D semiconductor-2D RGO nanocomposites in selective organic transformation fields.

Nanosized mesoporous anatase TiO_2 particles show outstanding photocatalytic performance in water remediation fields. Contrary to the conventional soft or hard template synthesis routes, uniform growth of mesoporous anatase TiO_2 nanospheres on graphene sheets was directly presented by a template-free self-assembly process, which easily achieved single crystal-like nanospheres and resulted in substantial improvement in photocatalytic removal of organic pollutant and hydrogen evolution [102]. Making full use of

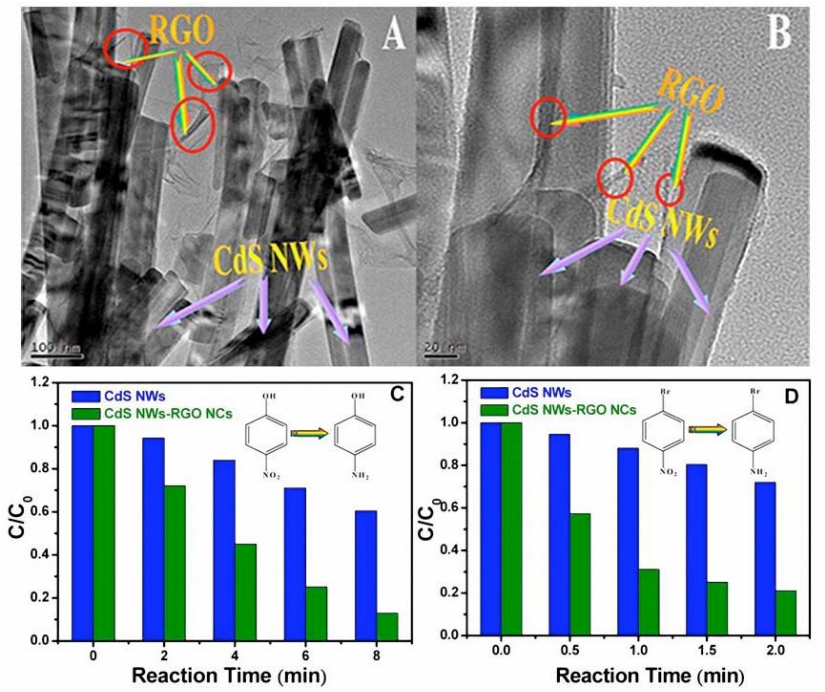

Fig. (6). Typical TEM images of the as-prepared samples of CdS NW−RGO NCs at different magnifications (A, B). Photocatalytic performance of the as-prepared CdS NWs and CdS NW-RGO NCs for aromatic nitro compound reduction under visible light irradiation (λ > 420 nm) with the addition of ammonium formate as a quencher for photogenerated holes and N_2 purge at room temperature in the aqueous phase: 4-nitrophenol (C); 1-bromo-4-nitrobenzene (D) [101].

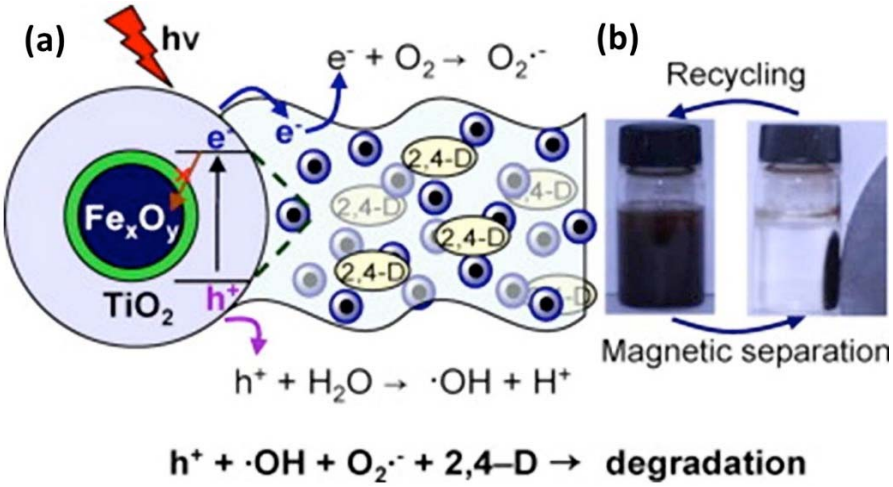

Fig. (7). Schematic illustration of the photodegradation mechanism of 2,4-D by magnetic TiO_2-graphene nanocomposite (a). Photograph of the magnetic separation and recycling process (b) [103].

graphene and TiO_2, a magnetic TiO_2-graphene photocatalyst was easily produced by combination of sol-gel and assembling processes [103]. Upon light irradiation, the charge separation of TiO_2 nanoparticles produces electrons (e^-) and holes (h^+). As good electron acceptors, negatively charged graphene sheets easily react with dissolved oxygen to yield superoxide anion radicals, who further react with hydrogen ions to produce hydroxyl radicals. As well, the holes are consumed by adsorbed water to form hydroxyl radicals. Thus, the adsorbed 2,4-D molecules on TiO_2-graphene active sites via π–π stacking or electrostatic force can be easily oxidized as shown in Fig. **7a**. Moreover, the catalyst can be fully recovered with the remaining removal efficiency of 97.7% for 2,4-D after 8 successive cycles (Fig. **7b**). In addition, it still kept a high removal efficiency of 95.6% towards 2,4-D even after one year, which makes it a promising candidate for pollutant removing applications. Ag-ZnO/reduced graphene oxide (Ag-ZnO/RGO) composite was also greenly prepared via a one-step hydrothermal process, in which the size of ZnO flowers is effectively controlled by Ag precursor and GO sheet. Thus, the hybrid nanostructure shows great photocatalytic and antibacterial activity [104]. More complex composites, such as $CoFe_2O_4$ and $ZnFe_2O_4$ nanoparticles, have also been studied for organic pollutant degradation. According to Wang's study, the combination of $CoFe_2O_4$ or $ZnFe_2O_4$ with graphene can lead to high degradation activity for organic pollutants, as well as easy recovery and recycling performance [105, 106].

Two dimensional nanoplatelets have also been introduced into graphene nanocomposites for adsorption and photo-degradation of organic pollutants [107-109]. In Peng's study, a new composite

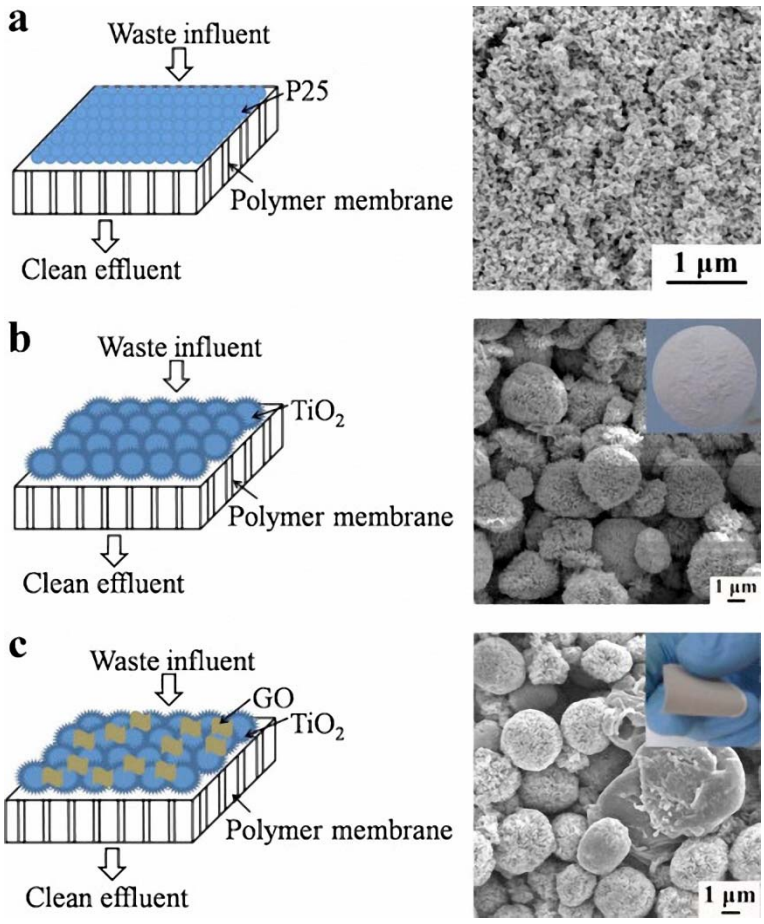

Fig. (8). Schematic diagram of P25 membrane (left side) and FESEM image of P25 membrane surface (right side) (a); schematic diagram of TiO_2 microsphere membrane (left side) and FESEM image of TiO_2 microsphere membrane surface (right side (inset: digital photo of TiO_2 microsphere membrane) (b); and schematic diagram of GO-TiO_2 membrane (left side) and FESEM image of GO-TiO_2 membrane surface (right side (inset: digital photo of GO-TiO_2 membrane) (c) [114].

consisting of silver phosphate (Ag_3PO_4) sub-microcrystals grown on layered molybdenum disulfide (MoS_2) and graphene (GR) hybrid was developed to be highly active for photocatalytic degradation of multi kinds of toxic organic pollutants [110]. With MoS_2/GR nanosheets serving as electron collectors, separation of photogenerated electron-hole pairs was greatly enhanced and the holes were more available for organic oxidation. Similarly, hybrid nanomaterials of reduced graphene oxide, zero-valent nickel, and NiAl-mixed metal oxides (RGO/Ni/MMO) have been synthesized by controllable thermal treatment of GO/layered double hydroxide (LDH) hybrid in N_2 [111]. With NiAl-LDHs being reduced into zero-valent Ni and NiAl-MMOs during calcination in the presence of GO substrate, this magnetic nanocomposite demonstrates outstanding adsorption and recycling abilities toward methyl orange removal.

A series of graphene sheets grafted three-dimensional $BiOBr_{0.2}I_{0.8}$ microspheres have been synthesized by a simple one-step solvothermal method, in which $BiOBr_{0.2}I_{0.8}$ microspheres composed of numerous nanoplatelets with a thickness of about 10 nm were uniformly dispersed on the surface of graphene [112]. The assembled $BiOBr_{0.2}I_{0.8}$/graphene composites exhibited excellent visible-light photocatalytic activity towards RhB and phenol, which was due to more effective charge transportations and separations, larger specific surface areas and the increased light absorption. Zou *et al.* reported the new role of GO as structure-directing and morphology-controlling agents in the nucleation and hydrothermal growth of heterostructured $Bi_2MoO_6/Bi_{3.64}Mo_{0.36}O_{6.55}$ composites [113]. Due to the optimal $Bi_2MoO_6/Bi_{3.64}Mo_{0.36}O_{6.55}$ phase ratio, unique morphology and structure, as well as the effective separation of photogenerated electrons and holes, the as-prepared 1% graphene-$Bi_2MoO_6/Bi_{3.64}Mo_{0.36}O_{6.55}$ composite exhibits the best photocatalytic degradation efficiency towards Rhodamine B. The worldwide concerning on clean water shortage has made the membrane technology a burning issue. In the work of Gao et al., a novel GO-TiO_2 composite membrane was obtained via the assembly of hierarchical GO-TiO_2 microspheres on the surface of a polymer filtration membrane (Fig. **8**) [114]. GO sheets play double roles of crosslinker for individual TiO_2 microspheres, and electron acceptor to improve photocatalytic activity of GO-TiO_2 membrane. Therefore, high permeate flux and photodegradation activity with no membrane fouling is realized in simultaneous water filtration and pollutant degradation.

3.2. Layered Double Hydroxides Based Nanocomposites

The anisotropy of a 2D nanosheet makes it an ideal 2D quantum system both for fundamental physical studies and synthesis of multi-functional materials, such as electronic, photonic, magnetic and mechanical materials [115]. A variety of nanocomposites [116], multilayer nanofilms [117], and hierarchical architectures [118], can be produced by the assembly or organization of charge-bearing

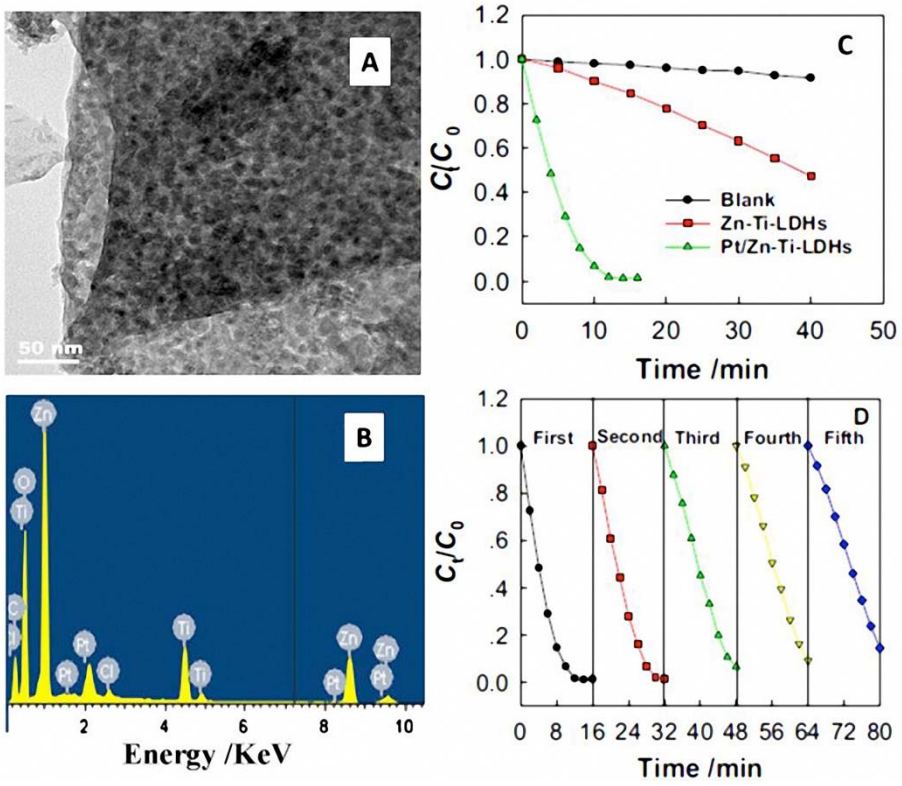

Fig. (9). TEM image (A) and the corresponding EDS spectrum (B) of Pt/Zn-Ti-LDHs. Photodegradation of RhB monitored as the normalized concentration vs irradiation time with the presence of different photocatalysts (C). Cycling runs in the photocatalytic degradation of RhB solution in the presence of Pt/Zn-Ti LDHs under simulated sunlight irradiation (D) [129].

inorganic nanosheets through different kinds of solution-based processing techniques (*e.g.*, LBL assembly, electrostatic self-assembly, and Langmuir-Blodgett method), which may have significant potentials for electronic, magnetic, optical, and catalytic applications. With the general formulation of $[M^{2+}_{1-x}M^{3+}_{x}(OH)_2]^{x+}(A^{n-})_{x/n}\cdot mH_2O$, layered double hydroxides (LDHs) are widely studied driven by the potential use for preparing CO_2 adsorbents, catalysts, or directly used as ion exchange hosts, drug delivery hosts, and as cement additives [119]. Due to their compositional flexibilities, exchangeable interlayer anions, large surface areas, ease of preparation and low cost, and "memory effect" (*i.e.*, the rehydration of calcined LDH), LDHs show great potentials as anionic adsorbents but low adsorption towards non-ionic organic compounds due to their hydrophilic nature [120, 121]. Thus, intercalation technique has been developed to change the surface hydrophobicity and improve adsorption affinity towards non-ionic organic pollutants [122, 123]. To enable effective dispersion, separation and guided movement of LDHs in solution phase, magnetic properties have also been introduced, where various types of LDHs consisting of magnetic cores such as Fe_3O_4, magnesium ferrite and cobalt ferrite have been prepared [118, 124]. Stable self-assembly of Fe_3O_4 nanoparticles on LDH nanocrystals has been achieved due to the strong electrostatic attraction between negatively charged magnetite nanoparticles and positively charged LDHs [125]. Moreover, the combination of 0D NPs and 2D nanoplatelets affords superior performance for organic dye treatments with fast adsorption kinetics and high adsorption capacity.

With the facile exfoliation and grafting properties of LDH single layers, both calcined and uncalcined LDHs are supposed to be effective supports for noble metal catalyst immobilization [126-128]. NanoPt intercalated Zn-Ti LDHs have been synthesized by ionic exchange and photochemical reduction method from Zn-Ti LDHs in H_2PtCl_6 solution (Fig. **9A**, **9B**) [129]. The combination of Zn-Ti-LDHs and Pt introduces some properties of Pt into photocatalysis such as excellent conductivity and controllability. Remarkable 17-fold enhancement in the degradation of rhodamine B reaction was observed on as-prepared Pt/Zn-Ti LDHs compared with pure Zn-Ti LDHs under simulated sunlight irradiation (Fig. **9C**, **9D**). The enhanced photocatalytic activity is ascribed to high specific surface (111.46 $m^2\ g^{-1}$), extended photoresponding range, negative shift in the flat-band potentials and the fast electron migration efficiency, which may effectively suppress the charge recombination. Bifunctional Ag/AgBr/Co-Ni-NO_3 LDH nanocomposites were facilely synthesized through an anion-exchange precipitation method [130]. Ag/AgBr nanoparticles were uniformly distributed on Co-Ni-NO_3 LDH sheets after adding $AgNO_3$ solution into Co-Ni-Br LDH suspension, which exhibited much higher adsorptive capacity (230 mg g^{-1}) towards methyl orange compared to Co-Ni-Br LDH, Ag/AgBr, and activated carbon. Higher photocatalytic activities towards dyes and phenol removal are achieved for the nanocomposites over Co-Ni-Br LDH and Ag/AgBr as well, making it promising for wide applications in wastewater treatment. Supported anatase-type TiO_2 nanoparticles have also been obtained by selective reconstruction of a Cu^{2+}, Mg^{2+}, Al^{3+}, Ti^{4+}-containing layered double hydroxide (CuMgAlTi-LDH), in which the skeleton Cu^{2+} ions enables photodegradation for MB. Due to the efficient photogenerated electrons/holes separation, the TiO_2/LDH heterojunction nanostructure provides new modes for load-type doped semiconductive photocatalysts with significantly improved photocatalytic activity [131].

With well-designed hierarchical nanocomposites constructed from 1D CNTs and 2D lamellar structures (*e.g.*, clay and LDHs)

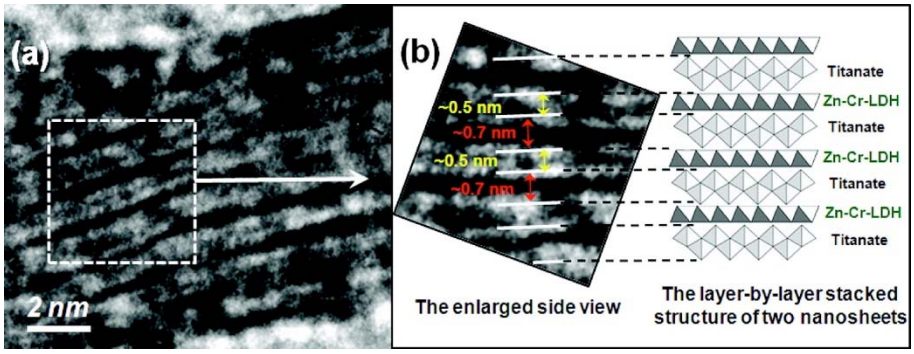

Fig. (10). Cross-sectional high-resolution TEM image of layered titanate/Zn_Cr-LDH nanohybrid (a) and its enlarged view and structural model (b) [133].

showing specific functions for unique applications, the uniform dispersion of nanoparticles in the matrix is always considered as a key issue. Nanocomposites of single/double-walled CNTs interlinked with 2D LDH flakes are fabricated, in which LDH is considered as an extraordinary catalyst for in-situ growth of high-quality CNTs [132]. The as-obtained CNT/calcined LDH nanocomposite acts as a new template for further construction of multi-functional materials in adsorption, catalysts, energy conversion and storage applications. The LBL self-assembly of oppositely charged 2D nanosheets of Zn-Cr LDH and layered titanium oxide easily leads to an ordered mesoporous nanohybrid with ordered in-plane atomic arrangements and electronic structures (Fig. **10**), thus achieving effective electronic coupling which is responsible for the strong visible-light absorption and depressed photoluminescence [133]. Therefore, the LBL assembly is a promising strategy for preparing chemically stable LDH-semiconductor hybrid materials with highly improved photocatalytic activity. Fe_3O_4@LDH@Ag/Ag_3PO_4 submicrosphere has been successfully obtained to show efficient visible-light activities towards photocatalytic degradation of organic pollutants with easy recyclability and reusability under an external magnetic field, being promising as a novel visible-light photocatalyst for water remediation [134].

4. THREE-DIMENSIONAL BUILDING BLOCK BASED NANOCOMPOSITES

Aerogel, a novel three dimensional structure, has attracted increasing concerns in applications of adsorption, catalysis, and energy storage, due to its high specific surface area (400-1200 $m^2 g^{-1}$), high porosity (> 80%), high mechanical strength, mesoporous structure (2-50 nm), and low cost [135-137]. These materials are basically obtained from the sol-gel polycondensation of certain organic monomers, such as resorcinol and formaldehyde [138, 139]. Mesoporous Fe/carbon aerogel (CA) structures with high specific surface areas of 487 $m^2 g^{-1}$ has been successfully developed via the carbonization of composite Fe_3O_4/phenol-formaldehyde resin structures, which were prepared using a hydrothermal process with the addition of phenol [140]. The mesoporous Fe/CA structures were further used for the adsorption of arsenic ions with a maximum arsenic-ion uptake of calculated 216.9 mg g^{-1}, much higher than that observed for other arsenic adsorbents. Besides, ferromagnetic behavior for the as-prepared mesoporous Fe/CA structures results in their easy separation and retrieval from solution under external magnetic fields.

Recently, porous inorganic hydrogels/aerogels are especially popular for applications in environmental and water remediation, such as energy storage, adsorption and catalysis [141]. However, it still remains an urgent challenge to inexpensively and efficiently create inorganic nanowire hydrogels/aerogels. An inorganic nanowire hydrogel/aerogel with high porosity was obtained via in-situ hydrothermal preparation of 1D nanowires [142]. The interconnecting nanowires with much longer length affords remarkably improved porosity, surface area, mechanical property, and decreased density (as low as 2.9 mg cm^{-3}) for catalysis or absorption. Kinetic and thermodynamic study show that optimal adsorption of azo-dye Orange II by titania aerogels occurs at pH = 2 with the strongest electrostatic interactions [143]. Moreover, the titania aerogel can be fully regenerated at pH = 11 and 30 ºC, demonstrating its efficient reusability and economic interest for environmental purposes. Similarly, a novel and green sol-gel process combined with supercritical extraction and drying has been applied for the preparation of nanostructured highly porous TiO_2/WO_3/Fe_3C aerogel composite photocatalysts, which definitely shows much superior photocatalytic capability than that of commercial Degussa P25 under visible light exposure [144]. With microcystins (MCs) causing severe environmental damages worldwidely, it is urgently required to seek an economical purification method to ensure the drinking water safety. Xia *et al.* novelly developed two nanoporous metal-organic framework MIL-100(Al) based xerogel and aerogel for highly efficient removal of the most toxic MC-LR in MC family with adsorption capacities reaching 6861 and 9007 mg g^{-1}, thus leading to much lower residual MC-LR concentration (0.093 mg L^{-1}) than the standard concentration (1 mg L^{-1}) for drinking water [145].

With the rapid development of carbonaceous materials, such as graphene and CNTs, carbonaceous materials have been increasingly applied in purification of waste water. An efficient way has been reported to fabricate MWNT-carbon hybrid hydrogels via a hydrothermal carbonization process, in which the gelation process is drastically promoted by the carbonaceous layers [146]. Ultralight 3D-graphene aerogels (GAs) are reported to be effective adsorbent for organic pollutants and electron transporter for photocatalysis as well [147]. Therefore, in-situ hydrothermal growth of well-dispersed mesoporous TiO_2 nanocrystals with (001) facets on GAs has been developed, in which glucose was used both as dispersant and linker [148]. With high electrical conductivity and strong interfacial interactions in 3D porous structures, TiO_2/GAs exhibit high photocatalytic activity and recyclability towards methyl orange pollutant. To be emphasized, metal ions, such as Ca^{2+}, Co^{2+}, Ni^{2+}, play key roles as skeleton, filler, and linker during the preparation of porously structured 3D GO-based materials, which may effectively improve the chemical cross-linking between graphene sheets [149]. By using Ni^{2+} ions as catalysts instead of the commonly used alkaline carbonates, Ni-doped graphene/carbon cryogels (NGCC) have been successfully prepared through the gelation process of

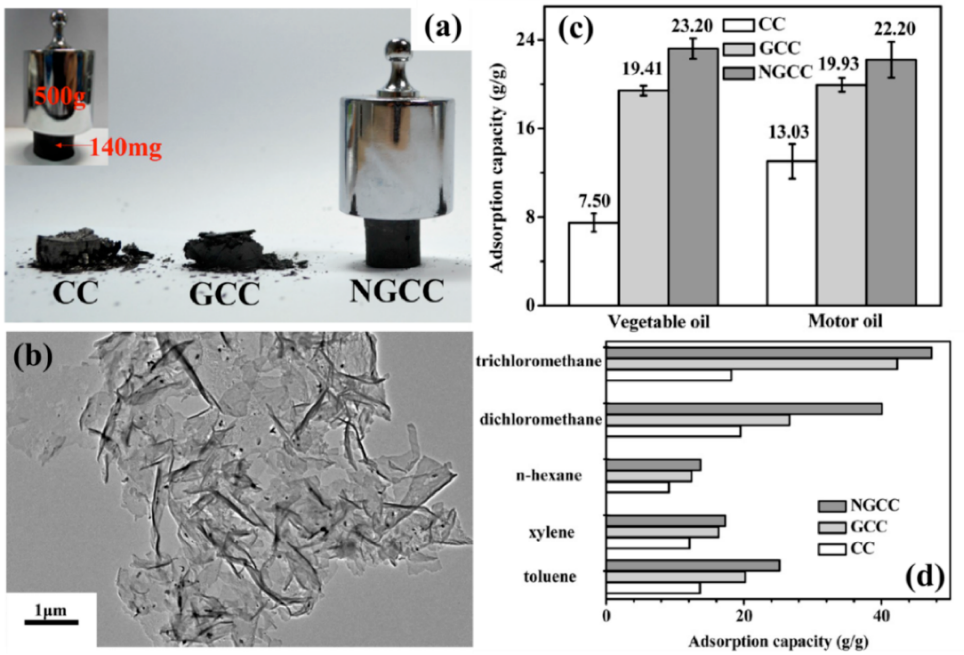

Fig. (11). (a) Digital photograph of carbon cryogel (CC), graphene/carbon cryogel (GCC), and NGCC with the same weight (90 mg) after loading with 200 g weight. Inset: 140 mg NGCC monolith enduring a weight of 500 g. (b) TEM image of NGCC. (c) The oil absorption capacity of CC, GCC, NGCC. (d) The organic solvent adsorption capacity of CC, GCC, and NGCC [150].

resorcinol and formaldehyde (RF) with GO [150]. The as-formed 3D interconnected structures with uniformly embedded Ni nanoparticles exhibit good mechanical properties, which can be attributed to the great strengthening of Ni^{2+}-induced crosslinking between GO and RF skeletons during the carbonization process (Fig. **11a**, **11b**). The unique porosity within the interconnected structures thus provides high extraction capability for oils and organic solvents with good recycling use (Fig. **11c**, **11d**), making the cryogels versatile candidates for pollutants elimination in water. A 3D network of carbon structures and a-FeOOH nanorods was also prepared from hydrothermal reduction of GO and CNTs [151]. With CNTs acting as a scaffold, the aerogels show excellent elastic modulus between 0.011 and 0.29 MPa. Moreover, the 3D graphene-CNTs aerogels with porous structures and low density (0.011-0.087 g cm^{-3}) exhibit high removal efficiency towards aqueous lead (230 and 451 mg g^{-1}), thus making them promising adsorbents for many environmental applications.

5. CONCLUSIONS AND OUTLOOK

Hierarchically organized nanocomposites derived from low-dimensional nanocarbon materials and metal/metal oxide (hydroxide) or semiconductors afford great potential to overcome various environmental problems, due to the fully extended or even synergistic advantages of all the component materials. However, the fabrication processes still face many severe challenges. As for low-dimensional building blocks, it is urgently necessary to address the stability and fine dispersion since they are critical to obtain nanocomposites that still keep the advantages of each nanocomponent. On the other hand, the interactions, homogeneity, and connectivity are major challenges during the construction of hierarchical architectures on macroscopic scale. This review is expected to provide useful information and inspire growing efforts in the design and preparation of hierarchically organized nanocomposites for versatile environmental remediation.

CONFLICT OF INTEREST

The authors confirm that this article content has no conflict of interest.

ACKNOWLEDGEMENTS

The authors are grateful for the financial support from the National Natural Science Foundation of China (51373037, 51125011, 51433001).

REFERENCES

[1] Kaur, A.; Gupta, U. A review on applications of nanoparticles for the preconcentration of environmental pollutants. *J. Mater. Chem.*, **2009**, *19*, 8279-8289.

[2] Wang, S.B.; Sun, H.Q.; Ang, H.M.; Tadé, M.O. Adsorptive remediation of environmental pollutants using novel graphene-based nanomaterials. *Chem. Eng. J.*, **2013**, *226*, 336-347.

[3] Khin, M.M.; Nair, A.S.; Babu, V.J.; Murugan, R.; Ramakrishna, S. A review on nanomaterials for environmental remediation. *Energy Environ. Sci.*, **2012**, *5*, 8075-8109.

[4] Chang, H.X.; Wu, H.K. Graphene-based nanocomposites: preparation, functionalization, and energy and environmental applications. *Energy Environ. Sci.*, **2013**, *6*, 3483-3507.

[5] Upadhyay, R.K.; Soin, N.; Roy, S.S. Role of graphene/metal oxide composites as photocatalysts, adsorbents and disinfectants in water treatment: A review. *RSC Adv.*, **2014**, *4*, 3823-3851.

[6] Zhang, T.C.; Surampalli, R.Y. *Nanotechnologies for Water Environment Application;* ASCE Publisher: Virginia, **2009**.

[7] Kharisov, B.I.; Rasika Dias, H.V.; Kharissova, O.V.; Manuel Jimenez-Perez, V.; Olvera Perez, B.; Munoz Flores, B. Iron-containing nanomaterials: Synthesis, properties, and environmental applications. *RSC Adv.*, **2012**, *2*, 9325-9358.

[8] Fu, F.; Dionysiou, D.D.; Liu, H. The use of zero-valent iron for groundwater remediation and wastewater treatment: A review. *J. Hazard. Mater.*, **2014**, *267*, 194-205.

[9] Sanchez, C.; Arribart, H.; Giraud Guille, M.M. Biomimetism and bioinspiration as tools for the design of innovative materials and systems. *Nat. Mater.*, **2005**, *4*, 277-288.

[10] Huebsch, N.; Mooney, D.J. Inspiration and application in the evolution of biomaterials. *Nature*, **2009**, *462*, 426-432.

[11] Zhao, M.Q.; Zhang, Q.; Huang, J.Q.; Wei, F. Hierarchical nanocomposites derived from nanocarbons and layered double hydroxides-properties, synthesis, and applications. *Adv. Funct. Mater.*, **2012**, *22*, 675-694.

[12] Yao, H.B.; Fang, H.Y.; Wang, X.H.; Yu, S.H. Hierarchical assembly of micro-/nano-building blocks: Bio-inspired rigid structural functional materials. *Chem. Soc. Rev.*, **2011**, *40*, 3764-3785.

[13] Li, S.; Luo, Y.; Lv, W.; Yu, W.; Wu, S.; Hou, P. Vertically aligned carbon nanotubes grown on graphene paper as electrodes in lithium-ion batteries and dye-sensitized solar cells. *Adv. Energy Mater.*, **2011**, *1*, 486-490.

[14] Lee, S.H.; Lee, D.H.; Lee, W.J.; Kim, S.O. Tailored assembly of carbon nanotubes and graphene. *Adv. Funct. Mater.*, **2011**, *21*, 1338-1354.

[15] Zhao, M.Q.; Huang, J.Q.; Zhang, Q.; Luo, W.L.; Wei, F. Improvement of oil adsorption performance by a sponge-like natural vermiculite-carbon nanotube hybrid. *Appl. Clay Sci.*, **2011**, *53*, 1-7.

[16] Moura, F.C.C.; Lago, R.M. Catalytic growth of carbon nanotubes and nanofibers on vermiculite to produce floatable hydrophobic "nanosponges" for oil spill remediation. *Appl. Catal. B.*, **2009**, *90*, 436-440.

[17] Zhang, W.D.; Xu, B.; Jiang, L.C. Functional hybrid materials based on carbon nanotubes and metal oxides. *J. Mater. Chem.*, **2010**, *20*, 6383-6391.

[18] Shulaker, M.M.; Hills, G.; Patil, N.; Wei, H.; Chen, H.Y.; Wong, H.S.P. Carbon nanotube computer. *Nature.*, **2013**, *501*, 526-530.

[19] Liu, J.W.; Liang, H.W.; Yu, S.H. Macroscopic-scale assembled nanowire thin films and their functionalities. *Chem. Rev.*, **2012**, *112*, 4770-4799.

[20] Iijima, S. Helical microtubules of graphitic carbon. *Nature*, **1991**, 354, 56-58.

[21] Wiśniewski, M.; Terzyk, A.P.; Gauden, P.A.; Kaneko, K.; Hattori, Y. Removal of internal caps during hydrothermal treatment of bamboo-like carbon nanotubes and application of tubes in phenol adsorption. *J. Colloid Interf. Sci.*, **2012**, *381*, 36-42.

[22] Wang, X.; Tao, S.; Xing, B. Sorption and competition of aromatic compounds and humic acid on multiwalled carbon nanotubes. *Environ. Sci. Technol.*, **2009**, *43*, 6214-6219.

[23] Yang, K.; Zhu, L.; Xing, B. Adsorption of polycyclic aromatic hydrocarbons by carbon nanomaterials. *Environ. Sci. Technol.*, **2006**, *40*, 1855-1861.

[24] Gotovac, S.; Song, L.; Kanoh, H.; Kaneko, K. Assembly structure control of single wall carbon nanotubes with liquid phase naphthalene adsorption. *Colloid. Surface A.*, **2007**, *300*, 117-121.

[25] Zou, M.Y.; Zhang, J.D.; Chen, J.W.; Li, X.H. Simulating adsorption of organic pollutants on finite (8,0) single-walled carbon nanotubes in water. *Environ. Sci. Technol.*, **2012**, *46*, 8887-8894.

[26] Wu, W.H.; Chen, W.; Lin, D.H.; Yang, K. Influence of surface oxidation of multiwalled carbon nanotubes on the adsorption affinity and capacity of polar and nonpolar organic compounds in aqueous phase. *Environ. Sci. Technol.*, **2012**, *46*, 5446-5454.

[27] Zhang, S.J.; Shao, T.; Kose, H.S.; Karanfil, T. Adsorption kinetics of aromatic compounds on carbon nanotubes and activated carbons. *Environ. Toxicol. Chem.*, **2012**, *31*, 79-85.

[28] Sun, Y.P.; Fu, K.; Lin, Y.; Huang, W. Functionalized carbon nanotubes: Properties and applications. *Acc. Chem. Res.*, **2002**, *35*, 1096-1104.

[29] Weng, B.; Liu, S.; Tang, Z.R.; Xu, Y.J. One-dimensional nanostructure based materials for versatile photocatalytic applications. *RSC Adv.*, **2014**, *4*, 12685-12700.

[30] Hull, R.V.; Li, L.; Xing, Y.; Chusuei, C.C. Pt nanoparticle binding on functionalized multiwalled carbon nanotubes. *Chem. Mater.*, **2006**, *18*, 1780-1788.

[31] Jiang, K.; Eitan, A.; Schadler, L.S.; Ajayan, P.M.; Siegel, R.W.; Grobert, N. Selective attachment of gold nanoparticles to nitrogen-doped carbon nanotubes. *Nano Lett.*, **2003**, *3*, 275-277.

[32] Xu, F.; Deng, S.; Xu, J.; Zhang, W.; Wu, M.; Wang, B. Highly active and stable Ni-Fe bimetal prepared by ball milling for catalytic hydrodechlorination of 4-Chlorophenol. *Environ. Sci. Technol.*, **2012**, *46*, 4576-4582.

[33] Yang, G.W.; Gao, G.Y.; Wang, C.; Xu, C.L.; Li, H.L. Controllable deposition of Ag nanoparticles on carbon nanotubes as a catalyst for hydrazine oxidation. *Carbon*, **2008**, *46*, 747-752.

[34] Jung, J.H.; Hwang, G.B.; Lee, J.E.; Bae, G.N. Preparation of airborne Ag/CNT hybrid nanoparticles using an aerosol process and their application to antimicrobial air filtration. *Langmuir*, **2011**, *27*, 10256-10264.

[35] Abou Asi, M.; Zhu, L.; He, C.; Sharma, V.K.; Shu, D.; Li, S. Visible-light-harvesting reduction of CO_2 to chemical fuels with plasmonic Ag@AgBr/CNT nanocomposites. *Catal. Today*, **2013**, *216*, 268-275.

[36] Lu, C.Y.; Tseng, H.H.; Wey, M.Y.; Chuang, K.H.; Kuo, J.H. Evaluating the potential of CNT-supported Co catalyst used for gas pollution removal in the incineration flue gas. *J. Environ. Manage.*, **2009**, *90*, 1884-1892.

[37] Yu, Y.; Yu, J.C.; Chan, C.Y.; Che, Y.K.; Zhao, J.C.; Ding, L. Enhancement of adsorption and photocatalytic activity of TiO_2 by using carbon nanotubes for the treatment of azo dye. *Appl. Catal. B.*, **2005**, *61*, 1-11.

[38] Li, Z.; Gao, B.; Chen, G.Z.; Mokaya, R.; Sotiropoulos, S.; Li Puma, G. Carbon nanotube/titanium dioxide (CNT/TiO_2) core–shell nanocomposites with tailored shell thickness, CNT content and photocatalytic/photoelectrocatalytic properties. *Appl. Catal. B.*, **2011**, *110*, 50-57.

[39] Silva, C.G.; Faria, J.L. Photocatalytic oxidation of benzene derivatives in aqueous suspensions: Synergic effect induced by the introduction of carbon nanotubes in a TiO_2 matrix. *Appl. Catal. B.*, **2010**, *101*, 81-89.

[40] Martínez, C.; Canle L, M.; Fernández, M.I.; Santaballa, J.A.; Faria, J. Kinetics and mechanism of aqueous degradation of carbamazepine by heterogeneous photocatalysis using nanocrystalline TiO_2, ZnO and multi-walled carbon nanotubes-anatase composites. *Appl. Catal.B.*, **2011**, *102*, 563-571.

[41] Wang, H.; Wang, H.L.; Jiang, W.F.; Li, Z.Q. Photocatalytic degradation of 2,4-dinitrophenol (DNP) by multi-walled carbon nanotubes (MWCNTs)/TiO_2 composite in aqueous solution under solar irradiation. *Water Res.*, **2009**, *43*, 204-210.

[42] Yu, H.; Quan, X.; Chen, S.; Zhao, H. TiO_2-multiwalled carbon nanotube heterojunction arrays and their charge separation capability. *J. Phys. Chem. C.*, **2007**, *111*, 12987-12991.

[43] Chen, L.C.; Ho, Y.C.; Guo, W.S.; Huang, C.M.; Pan, T.C. Enhanced visible light-induced photoelectrocatalytic degradation of phenol by carbon nanotube-doped TiO_2 electrodes. *Electrochim. Acta.*, **2009**, *54*, 3884-3891.

[44] Zhang, Y.C.; Utke, I.; Michler, J.; Ilari,G.; Rossell, M.D.; Erni, R. Growth and characterization of CNT-TiO_2 heterostructures. *Beilstein J. Nanotechnol.*, **2014**, *5*, 946-955.

[45] Liu, B.; Zeng, H.C. Carbon nanotubes supported mesoporous mesocrystals of anatase TiO_2. *Chem. Mater.*, **2008**, *20*, 2711-2718.

[46] Vietmeyer, F.; Seger, B.; Kamat, P.V. Anchoring ZnO particles on functionalized single wall carbon nanotubes: Excited state interactions and charge collection. *Adv. Mater.*, **2007**, *19*, 2935-2940.

[47] Zhang, W.D.; Jiang, L.C.; Ye, J.S. Photoelectrochemical study on charge transfer properties of ZnO nanowires promoted by carbon nanotubes. *J. Phys. Chem. C*, **2009**, *113*, 16247-16253.

[48] Feng, S.A.; Zhao, J.H.; Zhu, Z.P. The manufacture of carbon nanotubes decorated with ZnS to enhance the ZnS photocatalytic activity. *New Carbon Mater.*, **2008**, *23*, 228-234.

[49] Shankar, K.; Basham, J.I.; Allam, N.K.; Varghese, O.K.; Mor, G.K.; Feng, X. Recent advances in the use of TiO_2 nanotube and nanowire arrays for oxidative photoelectrochemistry. *J. Phys. Chem. C.*, **2009**, *113*, 6327-6359.

[50] Jennings, J.R.; Ghicov, A.; Peter, L.M.; Schmuki, P.; Walker, A.B. Dye-sensitized solar cells based on oriented TiO_2 nanotube arrays: Transport, trapping, and transfer of electrons. *J. Am. Chem. Soc.*, **2008**, *130*, 13364-13372.

[51] Tang, Z.R.; Li, F.; Zhang, Y.; Fu, X.; Xu, Y.J. Composites of titanate nanotube and carbon nanotube as photocatalyst with high mineralization ratio for gas-phase degradation of volatile aromatic pollutant. *J. Phys. Chem. C*, **2011**, *115*, 7880-7886.

[52] Zhu, K.; Vinzant, T.B.; Neale, N.R.; Frank, A.J. Removing structural disorder from oriented TiO_2 nanotube arrays: Reducing the dimensionality of transport and recombination in dye-sensitized solar cells. *Nano Lett.*, **2007**, *7*, 3739-3746.

[53] Liu, Z.; Zhang, X.; Nishimoto, S.; Murakami, T.; Fujishima, A. Efficient photocatalytic degradation of gaseous acetaldehyde by highly ordered TiO_2 nanotube Arrays. *Environ. Sci. Technol.*, **2008**, *42*, 8547-8551.

[54] Bae, J.; Han, J.B.; Zhang, X.M.; Wei, M.; Duan, X.; Zhang, Y. ZnO nanotubes grown at low temperature using Ga as catalysts and their enhanced photocatalytic activities. *J. Phys. Chem. C.*, **2009**, *113*, 10379-10383.

[55] Yousefi, R.; Jamali-Sheini, F.; Khorsand Zak, A.; Azarang, M. Growth and optical properties of ZnO-In_2O_3 heterostructure nanowires. *Ceram. Int.*, **2013**, *39*, 5191-51916.

[56] Balachandran, S.; Swaminathan, M. The simple, template free synthesis of a Bi_2S_3-ZnO heterostructure and its superior photocatalytic activity under UV-A light. *Dalton T.*, **2013**, *42*, 5338-5347.

[57] Gu, Y.Q.; Huang, J.G. Precise size control over ultrafine rutile titania nanocrystallites in hierarchical nanotubular silica/titania hybrids with efficient photocatalytic activity. *Chem. Eur. J.*, **2013**, *19*, 10971-10981.

[58] Qin, L.; Pan, X.X.; Wang, L.; Sun, X.; Zhang, G.L.; Guo, X.W. Facile preparation of mesoporous TiO_2(B) nanowires with well-dispersed Fe_2O_3 nanoparticles and their photochemical catalytic behavior. *Appl. Catal. B.*, **2014**, *150-151*, 544-553.

[59] Park, S.; Kim, S.; Kim, H.J.; Lee, C.W.; Song, H.J.; Seo, S.W. Hierarchical assembly of TiO_2-$SrTiO_3$ heterostructures on conductive SnO_2 backbone nanobelts for enhanced photoelectrochemical and photocatalytic performance. *J. Hazard. Mater.*, **2014**, *275*, 10-18.

[60] Xiao, F.X. Construction of highly ordered ZnO-TiO_2 nanotube arrays (ZnO/TNTs) heterostructure for photocatalytic application. *ACS Appl. Mater. Interfaces*, **2012**, *4*, 7055-7063.

[61] Xiao, F.X. Layer-by-layer self-assembly construction of highly ordered metal-TiO_2 nanotube arrays heterostructures (M/TNTs, M = Au, Ag, Pt) with tunable catalytic activities. *J. Phys. Chem. C.*, **2012**, *116*, 16487-16498.

[62] Xiao, F. Self-assembly preparation of gold nanoparticles-TiO_2 nanotube arrays binary hybrid nanocomposites for photocatalytic applications. *J. Mater. Chem.*, **2012**, *22*, 7819-7830.

[63] Xiao, F.; Wang, F.; Fu, X.; Zheng, Y. A green and facile self-assembly preparation of gold nanoparticles/ZnO nanocomposite for photocatalytic and photoelectrochemical applications. *J. Mater. Chem.*, **2012**, *22*, 2868-2877.

[64] Xiao, S.L.; Shen, M.W.; Guo, R.; Wang, S.Y.; Shi, X.Y. Immobilization of zerovalent iron nanoparticles into electrospun polymer nanofibers: Synthesis, characterization, and potential environmental applications. *J. Phys. Chem. C.*, **2009**, *113*, 18062-18068.

[65] Yang, D.J.; Kamienchick, I.; Youn, D.Y.; Rothschild, A.; Kim, I.D. Ultrasensitive and highly selective gas sensors based on electrospun SnO_2 nanofibers modified by Pd loading. *Adv. Funct. Mater.*, **2010**, *20*, 4258-4264.

[66] Pant, B.; Pant, H.R.; Barakat, N.A.M.; Park, M.; Jeon, K.; Choi, Y. Carbon nanofibers decorated with binary semiconductor (TiO_2/ZnO) nanocomposites for the effective removal of organic pollutants and the enhancement of antibacterial activities. *Ceram. Int.*, **2013**, *39*, 7029-7035.

[67] Ito, Y.; Takeuchi, T.; Tsujiguchi, T.; Abdelkareem, M.A.; Nakagawa, N. Ultrahigh methanol electro-oxidation activity of PtRu nanoparticles prepared on TiO_2-embedded carbon nanofiber support. *J. Power Sources*, **2013**, *242*, 280-288.

[68] Zhang, X.; Shao, C.; Zhang, Z.; Li, J.; Zhang, P.; Zhang, M. In situ generation of well-dispersed ZnO quantum dots on electrospun silica nanotubes with high photocatalytic activity. *ACS Appl. Mater. Interfaces*, **2011**, *4*, 785-790.

[69] Zhang, M.; Shao, C.; Guo, Z.; Zhang, Z.; Mu, J.; Cao, T. Hierarchical nanostructures of copper(II) phthalocyanine on electrospun TiO_2 nanofibers: Controllable solvothermal-fabrication and enhanced visible photocatalytic properties. *ACS Appl. Mater. Interfaces*, **2011**, *3*, 369-377.

[70] Li, C.J.; Wang, J.N.; Wang, B.; Gong, J.R.; Lin, Z.A novel magnetically separable TiO_2/$CoFe_2O_4$ nanofiber with high photocatalytic activity under UV-vis light. *Mater. Res. Bull.*, **2012**, *47*, 333-337.

[71] Ma, D.; Xin, Y.J.; Gao, M.C.; Wu, J. Fabrication and photocatalytic properties of cationic and anionic S-doped TiO_2 nanofibers by electrospinning. *Appl. Catal. B.*, **2014**, *147*, 49-57.

[72] Pant, B.; Pant, H.R.; Park, M.; Liu, Y.; Choi, J.W.; Barakat, N.A.M. Electrospun CdS-TiO_2 doped carbon nanofibers for visible-light-induced photocatalytic hydrolysis of ammonia borane. *Catal. Commun.*, **2014**, *50*, 63-68.

[73] Lee, J.S.; Kwon, O.S.; Jang, J. Facile synthesis of SnO_2 nanofibers decorated with N-doped ZnO nanonodules for visible light photocatalysts using single-nozzle co-electrospinning. *J. Mater. Chem.*, **2012**, *22*, 14565-14572.

[74] Ren, P.R.; Fan, H.Q.; Wang, X. Electrospun nanofibers of ZnO/$BaTiO_3$ heterostructures with enhanced photocatalytic activity. *Catal. Commun.*, **2012**, *25*, 32-35.

[75] Shang, M.; Wang, W.; Yin, W.; Ren, J.; Sun, S.; Zhang, L. General strategy for a large-scale fabric with branched nanofiber-nanorod hierarchical heterostructure: Controllable synthesis and applications. *Chem. Eur. J.*, **2010**, *16*, 11412-11419.

[76] Wang, R.Y.; Guo, J.; Chen, D.; Miao, Y.E.; Pan, J.S.; Tjiu, W.W.; Liu, T.X. "Tube brush" like ZnO/SiO_2 hybrid to construct a flexible membrane with enhanced photocatalytic properties and recycling ability. *J. Mater. Chem.*, **2011**, *21*, 19375-19380.

[77] Miao, Y.E.; Wang, R.Y.; Chen, D.; Liu, Z.Y.; Liu, T. X. Electrospun self-standing membrane of hierarchical SiO_2@γ-AlOOH (Boehmite) core/sheath fibers for water remediation. *ACS Appl. Mater. Interfaces*, **2012**, *4*, 5353-5359.

[78] Liu, Z.Y.; Miao, Y.E.; Liu, M.K.; Ding, Q.W.; Tjiu, W.W.; Liu, T.X. Flexible polyaniline-coated TiO_2/SiO_2 nanofiber membranes with enhanced visible-light photocatalytic degradation performance. *J. Colloid Interf. Sci.*, **2014**, *424*, 49-55.

[79] Allen, M.J.; Tung, V.C.; Kaner, R.B. Honeycomb carbon: A review of graphene. *Chem. Rev.*, **2009**, *110*, 132-145.

[80] Chen, D.; Tang, L.; Li, J. Graphene-based materials in electrochemistry. *Chem. Soc. Rev.*, **2010**, *39*, 3157-3180.

[81] Huang, X.; Yin, Z.; Wu, S.; Qi, X.; He, Q.; Zhang, Q. Graphene-based materials: Synthesis, characterization, properties, and applications. *Small*, **2011**, *7*, 1876-1902.

[82] Sreeprasad, T.S.; Maliyekkal, S.M.; Lisha, K.P.; Pradeep, T. Reduced graphene oxide-metal/metal oxide composites: Facile synthesis and application in water purification. *J. Hazard. Mater.*, **2011**, *186*, 921-931.

[83] Maliyekkal, S.M.; Sreeprasad, T.S.; Krishnan, D.; Kouser, S.; Mishra, A.K.; Waghmare, U.V. Graphene: A reusable substrate for unprecedented adsorption of pesticides. *Small*, **2013**, *9*, 273-283.

[84] Gupta, S.S.; Sreeprasad, T.S.; Maliyekkal, S.M.; Das, S.K.; Pradeep, T. Graphene from sugar and its application in water purification. *ACS Appl. Mater. Interfaces*, **2012**, *4*, 4156-4163.

[85] Sreeprasad, T.S.; Gupta, S.S.; Maliyekkal, S.M.; Pradeep, T. Immobilized graphene-based composite from asphalt: Facile synthesis and application in water purification. *J. Hazard. Mater.*, **2013**, *246-247*, 213-220.

[86] Sun, Y.P.; Li, X.Q.; Zhang, W.X.; Wang, H.P. A method for the preparation of stable dispersion of zero-valent iron nanoparticles. *Colloid. Surface A*, **2007**, *308*, 60-66.

[87] Phenrat, T.; Saleh, N.; Sirk, K.; Tilton, R.D.; Lowry, G.V. Aggregation and sedimentation of aqueous nanoscale zerovalent iron dispersions. *Environ. Sci. Technol.*, **2006**, *41*, 284-290.

[88] Karamani, A.A.; Douvalis, A.P.; Stalikas, C.D. Zero-valent iron/iron oxide-oxyhydroxide/graphene as a magnetic sorbent for the enrichment of polychlorinated biphenyls, polyaromatic hydrocarbons and phthalates prior to gas chromatography-mass spectrometry. *J. Chromatogr. A*, **2013**, *1271*, 1-9.

[89] Guo, J.; Wang, R.Y.; Tjiu, W.W.; Pan, J.S.; Liu, T.X. Synthesis of Fe nanoparticles@graphene composites for environmental applications. *J. Hazard. Mater.*, **2012**, *225-226*, 63-73.

[90] Fan, W.; Gao, W.; Zhang, C.; Tjiu, W.W.; Pan, J.S.; Liu, T.X. Hybridization of graphene sheets and carbon-coated Fe_3O_4 nanoparticles as a synergistic adsorbent of organic dyes. *J. Mater. Chem.*, **2012**, *22*, 25108-25115.

[91] Xiong, Z.; Zhang, L.L.; Zhao, X.S. Visible-light-induced dye degradation over copper-modified reduced graphene oxide. *Chem. Eur. J.*, **2011**, *17*, 2428-2434.

[92] Li, B.J.; Cao, H.Q.; Yin, J.F.; Wu, Y.A.; Warner, J.H. Synthesis and separation of dyes via Ni@reduced graphene oxide nanostructures. *J. Mater. Chem.*, **2012**, *22*, 1876-1883.

[93] Zhu, M.; Chen, P.; Liu, M. Highly efficient visible-light-driven plasmonic photocatalysts based on graphene oxide-hybridized one-dimensional Ag/AgCl heteroarchitectures. *J. Mater. Chem.*, **2012**, *22*, 21487-21494.

[94] Huang, Q.; Liu, W.; Peng, P.; Huang, W. Reductive dechlorination of tetrachlorobisphenol A by Pd/Fe bimetallic catalysts. *J. Hazard. Mater.*, **2013**, *262*, 634-641.

[95] Zhou, X.H.; Chen, Z.X.; Yan, D.H.; Lu, H.B. Deposition of Fe-Ni nanoparticles on polyethyleneimine-decorated graphene oxide and application in catalytic dehydrogenation of ammonia borane. *J. Mater. Chem.*, **2012**, *22*, 13506-13516.

[96] Li, Y.; Hu, Y.; Peng, S.; Lu, G.; Li, S. Synthesis of CdS nanorods by an ethylenediamine assisted hydrothermal method for photocatalytic hydrogen evolution. *J. Phys. Chem. C.*, **2009**, *113*, 9352-9358.

[97] Gao, Z.; Liu, N.; Wu, D.; Tao, W.; Xu, F.; Jiang, K. Graphene-CdS composite, synthesis and enhanced photocatalytic activity. *Appl. Surf. Sci.*, **2012**, *258*, 2473-2478.

[98] Stankovich, S.; Dikin, D.A.; Dommett, G.H.B.; Kohlhaas, K.M.; Zimney, E.J.; Stach, E.A. Graphene-based composite materials. *Nature*, **2006**, *442*, 282-286.

[99] Gao, P.; Liu, J.C.; Sun, D.D.L.; Ng, W. Graphene oxide-CdS composite with high photocatalytic degradation and disinfection activities under visible light irradiation. *J. Hazard. Mater.*, **2013**, *250-251*, 412-420.

[100] Linhui, Y.; Hong, R.; Yi, Z.; Danzhen, L. A facile solvothermal method to produce ZnS quantum dots-decorated graphene nanosheets with superior photoactivity. *Nanotechnology*, **2013**, *24*, 375601.

[101] Liu, S.Q.; Chen, Z.; Zhang, N.; Tang, Z.R.; Xu, Y.J. An efficient self-assembly of CdS nanowires-reduced graphene oxide nanocomposites for selective reduction of nitro organics under visible light irradiation. *J. Phys. Chem. C.*, **2013**, *117*, 8251-8261.

[102] Li, N.; Liu, G.; Zhen, C.; Li, F.; Zhang, L.; Cheng, H.M. Battery performance and photocatalytic activity of mesoporous anatase TiO_2 nanospheres/graphene composites by template-free self-assembly. *Adv. Funct. Mater.*, **2011**, *21*, 1717-1722.

[103] Tang, Y.H.; Zhang, G.; Liu, C.B.; Luo, S.L.; Xu, X.L.; Chen, L. Magnetic TiO_2-graphene composite as a high-performance and recyclable platform for efficient photocatalytic removal of herbicides from water. *J. Hazard. Mater.*, **2013**, *252-253*, 115-122.

[104] Raj Pant, H.; Pant, B.; Joo Kim, H.; Amarjargal, A.; Hee Park, C.; Tijing, L.D. A green and facile one-pot synthesis of Ag-ZnO/RGO nanocomposite with effective photocatalytic activity for removal of organic pollutants. *Ceram. Int.*, **2013**, *39*, 5083-5091.

[105] Fu, Y.; Chen, H.; Sun, X.; Wang, X. Combination of cobalt ferrite and graphene: High-performance and recyclable visible-light photocatalysis. *Appl. Catal. B.*, **2012**, *111-112*, 280-287.

[106] Fu, Y.; Wang, X. Magnetically separable $ZnFe_2O_4$-graphene catalyst and its high photocatalytic performance under visible light irradiation. *Ind. Eng. Chem. Res.*, **2011**, *50*, 7210-7218.

[107] Ai, Z.; Ho, W.; Lee, S. Efficient visible light photocatalytic removal of NO with BiOBr-graphene nanocomposites. *J. Phys. Chem. C.*, **2011**, *115*, 25330-25337.

[108] Li, B.; Cao, H.; Yin, G. $Mg(OH)_2$@reduced graphene oxide composite for removal of dyes from water. *J. Mater. Chem.*, **2011**, *21*, 13765-13768.

[109] Zhou, F.; Shi, R.; Zhu, Y. Significant enhancement of the visible photocatalytic degradation performances of γ-Bi_2MoO_6 nanoplate by graphene hybridization. *J. Mol. Catal. A*, **2011**, *340*, 77-82.

[110] Peng, W.C.; Wang, X.; Li, X.Y. The synergetic effect of MoS_2 and graphene on Ag_3PO_4 for its ultra-enhanced photocatalytic activity in phenol degradation under visible light. *Nanoscale*, **2014**, *6*, 8311-7.

[111] Yang, Z.; Ji, S.S.; Gao, W.; Zhang, C.; Ren, L.L.; Tjiu, W.W.; Liu, T.X. Magnetic nanomaterial derived from graphene oxide/layered double hydroxide hybrid for efficient removal of methyl orange from aqueous solution. *J. Colloid Interf. Sci.*, **2013**, *408*, 25-32.

[112] Liu, H.; Su, Y.; Chen, Z.; Jin, Z.T.; Wang, Y. Graphene sheets grafted three-dimensional $BiOBr_{0.2}I_{0.8}$ microspheres with excellent photocatalytic activity under visible light. *J. Hazard. Mater.*, **2014**, *266*, 75-83.

[113] Zou, J.P.; Ma, J.; Huang, Q.; Luo, S.L.; Yu, J.; Luo, X.B. Graphene oxide as structure-directing and morphology-controlling agent for the syntheses of heterostructured graphene-Bi_2MoO_6/$Bi_{3.64}Mo_{0.36}O_{6.55}$ composites with high photocatalytic activity. *Appl. Catal. B.*, **2014**, *156-157*, 447-455.

[114] Gao, P.; Liu, Z.Y.; Tai, M.H.; Sun, D.D.L.; Ng, W. Multifunctional graphene oxide-TiO_2 microsphere hierarchical membrane for clean water production. *Appl. Catal. B.*, **2013**, *138-139*, 17-25.

[115] Nakano, M.; Tsukazaki, A.; Ohtomo, A.; Ueno, K.; Akasaka, S.; Yuji, H. Correction: Electronic-field control of two-dimensional electrons in polymer-gated-oxide semiconductor heterostructures. *Adv. Mater.*, **2010**, *22*, 5081.

[116] O'Leary, S.; O'Hare, D.; Seeley, G. Delamination of layered double hydroxides in polar monomers: New LDH-acrylate nanocomposites. *Chem. Commun.*, **2002**, (14), 1506-1507.

[117] Li, L.; Ma, R.; Ebina, Y.; Iyi, N.; Sasaki, T. Positively charged nanosheets derived via total delamination of layered double hydroxides. *Chem. Mater.*, **2005**, *17*, 4386-4391.

[118] Li, L.; Feng, Y.; Li, Y.; Zhao, W.; Shi, J. Fe_3O_4 core/layered double hydroxide shell nanocomposite: Versatile magnetic matrix for anionic functional materials. *Angew. Chem. Int. Ed.*, **2009**, *48*, 5888-5892.

[119] Wang, Q.; O'Hare, D. Recent advances in the synthesis and application of layered double hydroxide (LDH) nanosheets. *Chem. Rev.*, **2012**, *112*, 4124-4155.

[120] Inacio, J.; Taviot-Guého, C.; Forano, C.; Besse, J.P. Adsorption of MCPA pesticide by MgAl-layered double hydroxides. *Appl. Clay Sci.*, **2001**, *18*, 255-264.

[121] Cardoso, L.P.; Valim, J.B. Study of acids herbicides removal by calcined Mg-Al-CO_3-LDH. *J. Phys. Chem. Solids.*, **2006**, *67*, 987-993.

[122] Bruna, F.; Celis, R.; Real, M.; Cornejo, J. Organo/LDH nanocomposite as an adsorbent of polycyclic aromatic hydrocarbons in water and soil-water systems. *J. Hazard. Mater.*, **2012**, *225-226*, 74-80.

[123] Bouraada, M.; Belhalfaoui, F.; Ouali, M.S.; de Ménorval, L.C. Sorption study of an acid dye from an aqueous solution on modified Mg-Al layered double hydroxides. *J. Hazard. Mater.*, **2009**, *163*, 463-467.

[124] Zhang, H.; Pan, D.; Zou, K.; He, J.; Duan, X. A novel core-shell structured magnetic organic-inorganic nanohybrid involving drug-intercalated layered double hydroxides coated on a magnesium ferrite core for magnetically controlled drug release. *J. Mater. Chem.*, **2009**, *19*, 3069-3077.

[125] Chen, C.; Gunawan, P.; Xu, R. Self-assembled Fe_3O_4-layered double hydroxide colloidal nanohybrids with excellent performance for treatment of organic dyes in water. *J. Mater. Chem.*, **2011**, *21*, 1218-1225.

[126] Zhu, J.Y.; Fan, H.; Sun, J.C.; Ai, S.Y. Anion-exchange precipitation synthesis of α-Ag_2WO_4/Zn-Cr layered double hydroxides composite with enhanced visible-light-driven photocatalytic activity. *Sep. Purif. Technol.*, **2013**, *120*, 134-140.

[127] Wang, J.; Zhao, L.; Shi, H.; He, J. Highly enantioselective and efficient asymmetric epoxidation catalysts: Inorganic nanosheets modified with α-Amino acids as ligands. *Angew. Chem. Int. Ed.*, **2011**, *50*, 9171-9176.

[128] Wypych, F.; Bail, A.; Halma, M.; Nakagaki, S. Immobilization of iron(III) porphyrins on exfoliated MgAl layered double hydroxide, grafted with (3-aminopropyl)triethoxysilane. *J. Catal.*, **2005**, *234*, 431-437.

[129] Chen, G.X.; Qian, S.M.; Tu, X.M.; Wei, X.Y.; Zou, J.P.; Leng, L.H. Enhancement photocatalytic degradation of rhodamine B on nanoPt intercalated Zn-Ti layered double hydroxides. *Appl. Surf. Sci.*, **2014**, *293*, 345-351.

[130] Fan, H.; Zhu, J.Y.; Sun, J.C.; Zhang, S.X.; Ai, S.Y. Ag/AgBr/Co-Ni-NO_3 layered double hydroxide nanocomposites with highly adsorptive and photocatalytic properties. *Chem. Eur. J.*, **2013**, *19*, 2523-2530.

[131] Lu, R.J.; Xu, X.; Chang, J.P.; Zhu, Y.; Xu, S.L.; Zhang, F.Z. Improvement of photocatalytic activity of TiO_2 nanoparticles on selectively reconstructed layered double hydroxide. *Appl. Catal. B.*, **2012**, *111-112*, 389-396.

[132] Zhao, M.Q.; Zhang, Q.; Jia, X.L.; Huang, J.Q.; Zhang, Y.H.; Wei, F. Hierarchical composites of single/double-walled carbon nanotubes interlinked flakes from direct carbon deposition on layered double hydroxides. *Adv. Funct. Mater.*, **2010**, *20*, 677-685.

[133] Gunjakar, J.L.; Kim, T.W.; Kim, H.N.; Kim, I.Y.; Hwang, S.J. Mesoporous layer-by-layer ordered nanohybrids of layered double hydroxide and layered metal pxide: Highly active visible light photocatalysts with improved chemical stability. *J. Am. Chem. Soc.*, **2011**, *133*, 14998-15007.

[134] Sun, J.C.; Fan, H.; Nan, B.; Ai, S.Y. Fe_3O_4@LDH@Ag/Ag_3PO_4 submicrosphere as a magnetically separable visible-light photocatalyst. *Sep. Purif. Technol.*, **2014**, *130*, 84-90.

[135] Moreno-Castilla, C.; Maldonado-Hódar, F.J. Carbon aerogels for catalysis applications: An overview. *Carbon*, **2005**, *43*, 455-465.

[136] Meena, A.K.; Mishra, G.K.; Rai, P.K.; Rajagopal, C.; Nagar, P.N. Removal of heavy metal ions from aqueous solutions using carbon aerogel as an adsorbent. *J. Hazard. Mater.*, **2005**, *122*, 161-170.

[137] Li, J.; Wang, X.; Huang, Q.; Gamboa, S.; Sebastian, P.J. Studies on preparation and performances of carbon aerogel electrodes for the application of supercapacitor. *J. Power Sources*, **2006**, *158*, 784-788.

[138] Long, D.H.; Zhang, J.; Yang, J.H.; Hu, Z.J.; Li, T.Q.; Cheng, G. Preparation and microstructure control of carbon aerogels produced using m-cresol mediated sol-gel polymerization of phenol and furfural. *New Carbon Mater.*, **2008**, *23*, 165-170.

[139] Al-Muhtaseb, S.A.; Ritter, J.A. Preparation and properties of resorcinol-formaldehyde organic and carbon gels. *Adv. Mater.*, **2003**, *15*, 101-114.

[140] Lin, Y.F.; Chen, J.L. Magnetic mesoporous Fe/carbon aerogel structures with enhanced arsenic removal efficiency. *J. Colloid Interf. Sci.*, **2014**, *420*, 74-79.

[141] Lee, J.M.; Choung, J.W.; Yi, J.; Lee, D.H.; Samal, M.; Yi, D.K. Vertical pillar-superlattice array and graphene hybrid light emitting diodes. *Nano Lett.*, **2010**, *10*, 2783-2788.

[142] Jung, S.M.; Jung, H.Y.; Fang, W.; Dresselhaus, M.S.; Kong, J. A facile methodology for the production of in situ inorganic nanowire hydrogels/aerogels. *Nano. Lett.*, **2014**, *14*, 1810-1817.

[143] Abramian, L.; El-Rassy, H. Adsorption kinetics and thermodynamics of azo-dye Orange II onto highly porous titania aerogel. *Chem. Eng. J.*, **2009**, *150*, 403-410.

[144] Li, H.; Sunol, S.G.; Sunol, A.K. Development of titanium-dioxide-based aerogel catalyst with tunable nanoporosity and photocatalytic activity. *Nanotechnology*, **2012**, *23*, 294012.

[145] Xia, W.; Zhang, X.M.; Xu, L.; Wang, Y.X.; Lin, J.H.; Zou, R.Q. Facile and economical synthesis of metal-organic framework MIL-100(Al) gels for high efficiency removal of microcystin-LR. *RSC Adv.*, **2013**, *3*, 11007-11013.

[146] Zhang, C.; Tjiu, W.W.; Liu, T.X. One-pot hydrothermal synthesis and reusable oil-adsorbing properties of porous carbonaceous monoliths using multi-walled carbon nanotubes as templates. *RSC Adv.*, **2013**, *3*, 14938-14941.

[147] Liu, F.; Chung, S.; Oh, G.; Seo, T.S. Three-dimensional graphene oxide nanostructure for fast and efficient water-soluble dye removal. *ACS Appl. Mater. Interfaces*, **2011**, *4*, 922-927.

[148] Qiu, B.C.; Xing, M.Y.; Zhang, J.L. Mesoporous TiO_2 nanocrystals grown in situ on graphene aerogels for high photocatalysis and lithium-ion batteries. *J. Am. Chem. Soc.*, **2014**, *136*, 5852-5855.

[149] Jiang, X.; Ma, Y.; Li, J.; Fan, Q.; Huang, W. Self-assembly of reduced graphene oxide into three-dimensional architecture by divalent ion linkage. *J. Phys. Chem. C.*, **2010**, *114*, 22462-22465.

[150] Wei, G.; Miao, Y.E.; Zhang, C.; Yang, Z.; Liu, Z.Y.; Tjiu, W.W., Liu, T.X. Ni-doped graphene/carbon cryogels and their applications as versatile sorbents for water purification. *ACS Appl. Mater. Interfaces*, **2013**, *5*, 7584-7591.

[151] Zhang, M.; Gao, B.; Cao, X.D.; Yang, L.Y. Synthesis of a multifunctional graphene-carbon nanotube aerogel and its strong adsorption of lead from aqueous solution. *RSC Adv.*, **2013**, *3*, 21099-21105.

Received: August 29, 2014 Revised: September 10, 2014 Accepted: January 10, 2015